TECHNISCHE UNIVERSITÄT
ILMENAU

Pontificia Universidad Católica del Perú

Escuela de Posgrado

Studies on Model-Following Control for a class of nonlinear MIMO systems using a quadrotor system as an example

Tesis para obtener el grado académico de
Maestro en Ingeniería de Control y Automatización que presenta:

Ing. Alberto Pablo Luna Rimayhuamán

Asesor PUCP:	**Prof. Dr.-Ing. Carlos Gustavo Pérez Zuñiga**
Co-Asesor TU Ilmenau:	**Prof. Dr.-Ing. Johann Reger**
	M.Sc. Julian Willkomm

Lima, 2025

Informe de similitud

Yo, **Carlos Gustavo Pérez Zuñiga**, docente de la Escuela de Posgrado de la Pontificia Universidad Católica del Perú, asesor de la tesis titulada **Studies on Model-Following Control for a class of nonlinear MIMO systems using a quadrotor system as an example**, del autor:

Alberto Pablo Luna Rimayhuaman

dejo constancia de lo siguiente:

- El mencionado documento tiene un índice de puntuación de similitud de 16 %. Así lo consigna el reporte de similitud emitido por el software Turnitin el 22/07/2025.
- He revisado con detalle dicho reporte y la Tesis o Trabajo de suficiencia Profesional, y no se advierte indicios de plagio.
- Las citas a otros autores y sus respectivas referencias cumplen con las pautas académicas.

Lugar y fecha:
Lima, 22/07/2025

Apellidos y nombres del asesor: **Pérez Zúñiga, Carlos Gustavo**	
DNI: 41864666	Firma: 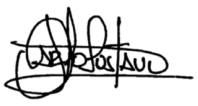
ORCID: 0000-0001-5946-1395	

Declaration

I hereby declare that I have written this thesis independently and have not used any other sources than those specified. All thoughts that have been taken either directly or indirectly from other sources have been explicitly identified as such. This thesis has not been submitted for credit in any other degree program or institution nor has it been previously published.

Pablo Luna
Ilmenau, 01 August 2023

Acknowledgements

I would like to express my deepest gratitude to my parents for the support, advice and constant encouragement throughout the course of my career. Their expertise and teaching have been instrumental for the direction and quality of my life. This work also goes for my brother and sister for being attentive for the steps of this challenging journey. I am also thankful to Dr. Reger and Msc. Julian Willkomm for providing the resources and guidance that enabled me to carry out this work.

Abstract

This master thesis is dedicated to the design and simulation of a model following controller for a quadrotor underactuated system. First, the quadrotor is modeled as a nonlinear Multi-Input Multi-Output (MIMO) system in affine form with four inputs (torques and thrust) and for outputs (three axis position and yaw angle). This was made by kinematics and Newton-Euler dynamics formulation. For the design, the model following control is composed by a Model Control Loop (MCL) where an idealized nominal plant model is considered. In this stage the special case of dynamic extension for MIMO systems is considered to obtain the decoupling matrix nonsingular and achieve full relative degree, then the augmented system is transformed in a Byrnes-Isidori-form so feedback linearization technique with state feedback gain can be applied for a reference trajectory. Hence, a second controller that operates on the real plant is designed. This is called a Process Control Loop (PCL). The nonlinear system is considered with external disturbances and is modeled based on the error dynamics between the process output and the nominal model output. The control is designed applying feedback linearization with high-gain state feedback with bounded uncertainty for the robustness. The obtained control law is feedforwarded by the control input of the MCL to make the outputs of the process follow the outputs of the MCL. The control system was compared with a single-loop state feedback pole placement design. The simulations demonstrated the stability under uncertainties and better trajectory tracking.

Kurzfassung

Diese Masterarbeit widmet sich dem Entwurf und der Simulation eines Model Following Controllers für ein unteraktuiertes Quadrotor-System. Zunächst wird der Quadrotor als nichtlineares MIMO (Multi-Input Multi-Output) System in affiner Form mit vier Eingängen (Drehmomente und Schub) und vier Ausgängen (Position entlang der drei Achsen und Gierwinkel) modelliert. Dies wird durch kinematische und Newton-Euler-Dynamikformulierung erreicht. Für den Entwurf besteht der Model Following Control aus einer Model Control Loop (MCL), in der ein idealisiertes Modell des Prozesses berücksichtigt wird. Während dieses Schrittes wird der spezielle Fall der dynamischen Erweiterung für MIMO-Systeme betrachtet, um die Entkopplungsmatrix nicht-singulär zu machen und den vollen relativen Grad zu erreichen. Anschließend wird das erweiterte System in eine Byrnes-Isidori-Form transformiert, so dass die Feedback-Linearisierungstechnik mit Zustandsrückführungsverstärkung auf eine Referenztrajektorie angewendet werden kann. Daher wird ein zweiter Controller entworfen, der am eigentlichen Prozess arbeitet. Dies wird als Process Control Loop (PCL) bezeichnet. Das nichtlineare System wird unter Berücksichtigung von externen Störungen modelliert, basierend auf der Fehlerdynamik zwischen der Prozessausgabe und der Ausgabe des nominalen Modells. Die Regelung wird unter Anwendung der Feedback-Linearisierung mit high-gain Zustandsrückführungsverstärker und begrenzter Unsicherheit für die Robustheit entworfen. Das erhaltene Regelgesetz wird durch die Steuereingabe der MCL vorwärts geführt, um die Ausgänge des Prozesses den Ausgängen der MCL zu folgen. Das Regelungssystem wurde mit einer Einzelschleifensteuerung mit Polplatzierung verglichen. Die Simulationen zeigten die Stabilität unter Unsicherheiten und eine bessere Trajektorienverfolgung.

Resumen

La tesis de maestría está dedicada al diseño y simulación de un controlador por seguimiento de modelo (MFC por sus siglas en inglés) para un sistema subactuado de cuadrirrotor. En primer lugar, el cuadrirrotor es modelado como un sistema no lineal afin de múltiples entradas y múltiples salidas (MIMO, por sus siglas en inglés) con cuatro entradas (tres torques y empuje) y cuatro salidas (posición en tres coordenadas y ángulo de guiñada). Esto fue elavorado mediante la formulación de cinemática y dinámica de Newton-Euler. Para el diseño, el control por seguimiento de modelo está compuesto por un bucle de control basado en el modelo (MCL por sus siglas en inglés) en donde es considerado el modelo nominal del sistema ideal. En esta fase es considerado el caso especial de la dinámica extendida para sistemas MIMO con el fin de obtener la matriz de desacoplo no singular y alcanzar el grado relativo completo, luego el sistema extendido es transformado en la forma de Byrnes-Isidori para que la técnica de linealización por realimentación con ganancia por realimentación de estados pueda ser aplicada para trayectorias de referencia. En segundo lugar, un segundo controlador que opera con el proceso real es diseñado. Este diseño es llamado control basado en el proceso (PCL por sus siglas en inglés). El sistema nolineal es considerado con perturbaciones externas y es modelado basado en la dinámica del error entre la salida del proceso y la salida del modelo nominal. Además, el controlador es diseñado aplicando la ténica de linealización por realimentación con realimentación de estados de alta ganancia con incertidumbre acotada para garantizar robustez. La ley de control obtenida es anticipada por la señal de control del bucle de control de modelo para hacer que la salida del proceso siga a la señal de salida del modelo. Finalmente, el sistema de control es comparado con la técnica de diseño por ubicación de polos mediante realimentación de estados. Las simulaciones demostraron la estabilidad bajo incertidumbre y mejor seguimiento de trajectorias.

Contents

List of Figures

List of Tables

Chapter 1

Introduction

1.1. Motivation

An Unmanned Aerial Vehicle (UAV), also known as a drone, is an aircraft that operates without a pilot onboard that can be remotely controlled or have an autonomous flight [14] [55]. With the advancement of technology drones have been applied in the fields of mining, agriculture, forestry, archaeology, architecture and even in construction industry [5].

They have the capability to integrate various sensors for data collection; for instance, cameras, LiDAR, multispectral sensors or specialized instruments for atmospheric measurements [72][34][81]. UAVs can also provide assistance for environmental monitoring. They are utilized for the mapping and surveillance of forested areas. Due to that work, researchers can monitor wildlife, climate change and human activities in the environment [68][43][29]. These aircraft play important role in agricultural research; for example, with specific sensors they can detect diseases, monitor crop health, improve the enhancement of irrigation and fertilization strategies [18] [27]. In the area of civil engineering and infrastructure, UAVs are utilized for inspection constructions, buildings, bridges. They can inspect these structures without the help of human intervention [12][21]. In the context of transportation applications concepts, drones are being used for traffic management, checking congestion providing real-time information [49][52].

UAVs have also gained important consideration in control system algorithms research area. They were used as testbeds for developing and testing control techniques to improve flight stability, trajectory following or tracking, and moveability [80]. Researchers have explored into state of the art in control methodologies to investigate the potential of UAVs; for instance, nonlinear control, adaptive control, sliding mode control and backstepping control to improve the performance of these aircraft. These control system algorithms are designed to overcome the complexities associated with nonlinear dynamics, uncertainties, and external disturbances affecting the flight of the drone [25][56][35][65]. By taking UAVs as test platforms, researchers can investigate and validate the performance of these algorithms enhancing the advancements

in autonomous flight, collision avoidance or swarm of multiple UAVs. The integration of control system algorithms in UAVs brings possibilities for safe, efficient, and intelligent aerial operations in numerous areas of expertise.

1.2. Quadrotor: general view

There are four categories UAVs were divided: fixed wing UAV, UAVs based on rotary wing and flapping wing configuration, UAVs based on hybrid wing and gas envelope-based UAVs. The quadrotor is a kind of Unmanned Aerial Vehicle (UAV) that belongs to the category of "rotating and flapping" because of its Vertical Take Off and Landing (VTOL) ability. Its basic components are a frame with four motors, propellers, gyroscopes, accelerometers, GPS and a control system board. The movement of the aircraft depends on the change of velocities of its motors [40] [32]. The operational framework in this aerial technology has similarity with the fundamental principle of helicopters, in which both of them achieve hovering movement by creating a downward force of air [9]. A real quadrotor is shown in Figure 1.1 where the physical components can be observed.

Figure 1.1: Typical quadrotor that is used for testbed of control algorithms [9].

VTOL aircraft which have the ability to hover and low-speed fly are helpful in isolated zones and also in places with reduced space for landing compared to the fixed wing UAVs which need devices for landing and take-off that are not accessible in cities and distant areas [46]. The research field for this kind of UAV have been grown through time. Their control performance has been subject of investigation in many studies most related to autonomous flight, also mentioned in the previous introduction section [77]. Quadrotors operate without the need for sophisticated mechanical linkages to control the movement of their rotors This are advantages over other UAV VTOL like a helicopter. Additionally, employing four separate rotors leads to their reduced diameters in comparison to the single main rotor commonly found in helicopters. This reduction in rotor size results in a decrease in the amount of stored kinetic energy associated with each individual rotor. A disadvantage is that the quadrotor design is made to operate with four rotors or actuators (which will be named control inputs in the modeling chapter) to control the six movements of translation and rotation (six degrees

of freedom) independently. This represents an underactuated system, because the number of control inputs is smaller than the degrees of freedom [48] [20]. Nevertheless, due to its lightweight components and low-cost, these aircraft were considered as testbeds for different control algorithms [8].

1.3. State of the art

The field of quadrotor control systems has witnessed significant advancements and research, leading to developments in autonomous flight, stability, and maneuverability. This is achieved because of the control algorithm design implemented. This subsection provides a summary of the state of the art research in quadrotor control, highlighting the areas of innovative methodologies, and significant contributions.

In the realm of engineering, a quadrotor can be characterized as a system with nonlinearity, coupled dynamics, multivariable underactuated behavior which they are complex to handle [19]. Linear control methods; for instance, proportional integral derivative (PID) control was applied in [59] in which the controller demonstrates the ability to achieve stability of this complicated system; nevertheless, the performance of the flight is impacted by the existence of external disturbances and the values of the implemented controller parameters are different from the simulation parameters. External disturbances were no considered in the mathematical model and it was linearized around an equilibrium point.

In order to deal with those problems, nonlinear control methods were implemented. Feedback linearization is one of these techniques. The fundamental concept underlying this methodology involves the algebraic transformation of the dynamics of a nonlinear system into either a fully or partially linear representation, therefore allowing designers the application of linear control techniques [67]. The employment of this method has shown results in robotics, helicopter flight control and aircraft performance. Furthermore, in the field of unmanned aerial vehicles (UAVs), feedback linearization control strategies were applied to quadrotor flight control. In [66] the authors proposed a controller design for the quadrotor combining a feedback linearization nonlinear technique and a linear quadratic regulator (LQR) control strategy, instead of linearization of the model, in order ot stabilize the attitude dynamics of the aircraft. Through numerical simulations the control system's stability and robustness under nominal conditions were validated. Additionally, flight tests with the addition of a bounded disturbance showed the controller's successful performance. Another contribution of this technique was showed in [10] where a feedback linearization with model predictive control scheme was developed for guiding the quadrotor along desired trajectories. By this method the nonlinear state-space model was transformed into a linear system while preventing round-off errors associated with Taylor series approximations. Additionally, a disturbance estimator was implemented for estimating and compensating the external disturbances, thereby guaranteeing error BIBO stability. The proposed control algorithm was evaluated through numerical simulations, examining tracking performance for the quadrotor in different scenarios even under constant or continuous disturbances. Nevertheless, the designed was

developed until simulation stage. The authors considered the implementation on actual quadrotors for the future work.

Another notable approach for quadrotor control is backstepping control. Backstepping control is a control technique used for stabilizing nonlinear dynamical systems by recursively designing control laws for each subsystem defined by virtual error variables which are stabilized by a Lyapunov function. The control process is completed when the final external control is attained [24]. Several researchers have explored the application of backstepping control in quadrotors with the objective of improving stability, trajectory tracking and robustness. For instance, in [82] the authors proposed a control strategy based two subsystems called inner and outer loops to elude the straightforward design of underactuated control inputs for a quadrotor. For the outer loop control laws were designed to provide pitch and roll angles as references inputs for the inner loop so that the position control inputs can be designed. This architecture is depicted in Figure 1.2.

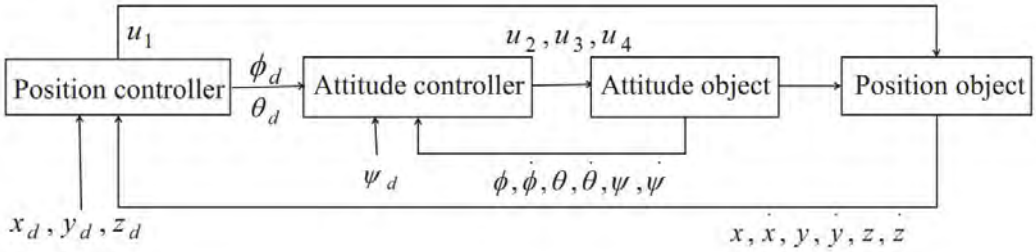

Figure 1.2: Inner outer control structured for quadrotor. The control inputs u_1, u_2, u_3 and u_4 were all designed by backstepping method. Source: [82].

Simulation results showed that the roll and pitch angle are able to follow the reference angles generated by the outer loop. So the tracking errors of position and attitude regularized to zero. Therefore, the quadrotor is can follow a predefined trajectory. The previous designs assumed a constant mass of the quadrotor; however, when these aircraft are used for agricultural applications, payload transport or environmental monitoring their mass can change drastically. That can affect the flight and therefore the performance of the drone. To solve that problem authors in [83] presented a backstepping adaptive controller adding an observer for real time mass estimation of a quadrotor with slow-varying mass during flight. Simulation results demonstrate that the hovering control can be achieved with a slight average error range equivalent to 2% of its own mass by using the proposed design.

Keeping the context of uncertainties and disturbances affecting the system there is other nonlinear control strategy called sliding mode control which is a robust control method that has gained attention due to the capability to handle uncertainties and disturbances. Sliding Mode Control (SMC) is a form of Variable Structure Control (VSC) that employs a discontinuous control signal to take the system onto a sliding surface in the state space. Once the system is on the switching surface, the resulting response behavior depends on the gradients of the switching plane and the control rapidly switches to maintain the states on the surface and drive them to desired states, such as the origin. This attractive feature ensures

robust performance even in the presence of uncertainties, parameters variation, making the technique a promising approach in modern control theory [78] [64]. Quadrotor control is a difficult problem when considering external disturbances, parameter uncertainties during flight. Due to these challenging tasks authors in [64] chose the sliding mode control for the translational and rotational dynamics of a quadcopter system. The robustness design was tested by simulations including lag dynamics on the actuators, then a second analysis the inertia, arm length and mass parameters of the aircraft had a parametric uncertainty of 20 - 50 %; finally, for unknown external disturbances gaussian normal noice was taken account. The results showed that the quadcopter can be stabilized by the design control at the reference position and altitude.

The principal drawback in sliding mode control is the so-called chattering problem in the control signal that means high frequency variation signal that the actuator should receive; nevertheless, designers found solutions to solve this problem; for example, in [2] authors designed a chattering suppressed controller for the attitude dynamics of a spacecraft taking account uncertainty and disturbances. The controller technique applied was a second order sliding mode control (SOSMC) which in closed loop simulations it showed that the main objective is accomplished bye suppressing the chattering in control. Other higher-order sliding mode control method that effectively deals with chattering is the super twisting method. In the publication in [7] authors proposed a robust super twisting (RST) terminal sliding mode control (RST-TSMC) in discrete-time domain to ensure trajectory tracking of a quadrotor with high accuracy in presence of external disturbances. The control structured was also developed in inner outer loops where Lyapunov function candidates were considered in order to guarantee the asymptotic stability. In the simulations results it is shown that the control inputs are smooth and did not obtain problems with chattering. The chattering issue is resolved by substituting the discontinuous term in the control law with a continuous function such as the hyperbolic tangent function.

Due to the tracking performance with robustness and disturbance rejection Model Following Control (MFC) has been applied to nonlinear dynamical systems. This method represents a structure of two-degree-of-freedom that consists of the Model Control Loop (MCL) where the nominal system is considered as reference system and the Process Control Loop (PCL) where the actual plant with disturbances are considered. Classic linear techniques are regularly used as controllers in both loops. Researchers have focused on and applied this control architecture. In [53] authors used the structure of the MFC to regularize the speed of a permanent magnet synchronous motor (PMSM). For the MCL a proportional controller is designed and for the PCL a PD-I fuzzy controller with adjusting parameters. The simulations and experimental tests of the control system showed robustness and stability when they changed the load torque and modify the moment of inertia. For the the boost-pressure reference-tracking of an exhaust-gas turbo-charger the authors in [74] designed a MFC. They elaborated a state feedback gain in the MCL based on a local model network (LMN) and for the PCL they developed a PI controller. For the simulations they compared the whole system with an inverse feedforward strategy with H_∞ for the PCL. It showed that the MFC with PI controller had good performance. A study where nonlinear techniques were applied in the MFC structure is found in [76]. Authors designed a target value control strategy for the

MCL then consider a high-gain state feedback with bounded uncertainty for the robustness in the PCL in order to reduce control action. In both loops partial feedback linearization was utilized.

1.4. Thesis objectives

1.4.1. General objective

The general objective is to design a model following controller for a nonlinear MIMO (Multi-Input Multi-Output) system. The structured is based on two control subsystems: model control loop (MCL) and a process control loop (PCL). Feedback linearization control law is used for both subsystems based on error dynamics. In this work it is considered the special case of dynamic extension for MIMO systems to obtain the decoupling matrix nonsingular and achieve full relative degree. For robustness performance, uncertainty analysis is developed for the complete system.

1.4.2. Specific objectives

The subsequent topics are addressed to accomplish the main objective:

- State of the art regarding model following control techniques applied to nonlinear systems.
- Analysis of quadrotor MIMO nonlinear mathematical model.
- MIMO feedback linearization via dynamic extension for the nominal dynamics.
- Design a nominal control law for set-point tracking and trajectory tracking. This controller shall be implemented in the model control loop.
- Robust control design (e.g. high-gain control). This robust controller shall be used in the process control loop and diminish the influence of model uncertainties.
- Evaluation of the model following control stability considering the model uncertainty.
- Simulation of the model and process control loop designs.
- Comparison with a single-loop feedback design.

1.5. Overview of present work

The structured of the present work is outlined in the following manner:

In chapter two the quadrotor's mathematical model is derived. It starts with the description of the system explaining how the quadrotor works as six degrees of freedom (6DOF) in the physical world. The mathematical foundations is explained. The kinematics of the quadrotor as rigid body is analyzed. Then, the nonlinear dynamics is deployed explaining the physical forces of the rotational and translational movements. The inputs and the outputs of the MIMO (Multi-Input Multi-Output) system are indicated. Finally, the quadrotor model is described by state space vector differential equations.

The control design is elaborated in chapter three. The control strategy is the model following control. It is composed of a two-loop control configuration: the model control loop (MCL) and the process control Loop (PCL). Feedback linearization and high gain feedback techniques are applied for stability problem. Finally, the analysis of disturbance is considered for robustness performance.

In chapter four, the simulations and results are presented bye software for validation purpose of the two loop structures mentioned before. A trajectory reference is presented to exhibit the controller's performance under flight condition with and without wind disturbance.

In chapter five, the conclusions and future work of the thesis are presented.

Chapter 2

Mathematical model of the quadrotor

In this chapter the quadrotor's mathematical model is developed. First, the quadrotor is described as a six degrees of freedom dynamic system; assumptions are considered for the model, so that the Newton-Euler rigid body analysis can be applied by the equations of kinematics and dynamics. Finally, the nonlinear mathematical model of the quadrotor is obtained.

2.1. Quadrotor: System description

The quadrotor is an specific type of aerial robot which consists of a fixed frame, four motors which are the actuators, with four propellers fixed to each motor's shaft, an electronic board where there are the control and communication system; sensors and any other electronic device according to the application.

There are two kind of frame-configurations so the quadrotor can have an indicator of the front when it is flying: the plus (+) where one motor is the head of the quadrotor and the cross (x) configuration where two motors are the head of the aircraft [60] [50]. A representation of these frames is shown in Figure 2.1. For the present work, the plus (+) configuration was chosen because a coordinate reference had to be aligned with the head of the quadrotor.

According to Newton's third law of motion for every action, there is an identical and opposite reaction. For the quadrotor case when the propellers rotate they generate force pushing the air downwards. The reaction will generate an opposite force making the quadrotor elevate [60]. This is made when the four motors have the same speed.

As shown in the image below numbers were assigned to each motor so they can be identified for the modeling. Two opposite propellers of the quadrotor spin clockwise and on the contrary the other two spin counterclockwise [22]. For this case the propellers in the first and third motors spin in clockwise and the propellers in the second and fourth motors spin in counterclockwise.

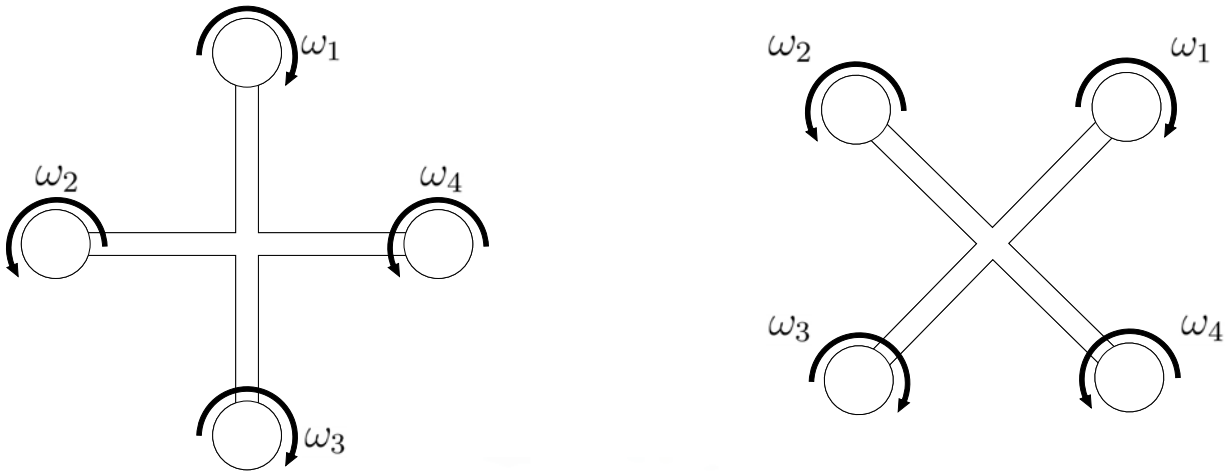

(a) + configuration (b) X configuration

Figure 2.1: Quadrotor configuration

It is the same spinning way for the cross configuration.

when a motor spin it generates a torque and it influences the movement of the quadrotor. According of the configurations in Figure 2.2 when the four motors have the same speed there will be a torque distribution, so the quadrotor will be in hover position and when the speed of the motors increase or decrease the aircraft will go up or down in vertical way [60] [22]. This is the throttle movement. So when the motors change their velocities the quadrotor will tilt and move front side to side. These are other movements are called roll, pitch and yaw [37]. This types of motions are shown in Figure 2.2 and this means that the quadrotor has movements along the x, y and z coordinates and also it rotates with respect of those coordinates. Due to those statements the quadrotor is said to have six degrees of freedom (6DOF) [39].

When the quadrotor change the speed of its motors the roll, pitch and yaw angular movements are made. Follow the configuration of Figure 2.2. The roll movement is created by increasing the speed of the first motor and decreasing the speed of the third motor by the same amount while the other motors keep the same speed. On the other hand, for the pitch movement the motor 2 has to increase the speed and motor 4 has to decrease the speed while other motors keep the same speed. For the yaw movement motors 1 and 3 have to increase their speed and the motors 2 and 4 have to decrease their speed generating a rotation torque with respect the z axis [31] [71] [60].

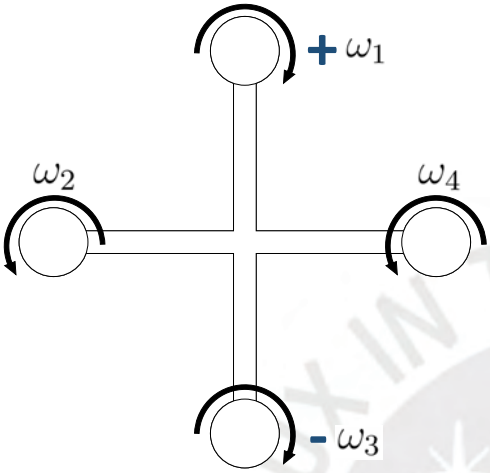

(a) Roll movement

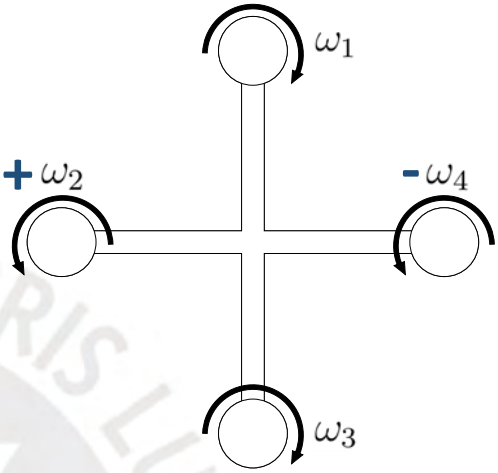

(b) Pitch movement

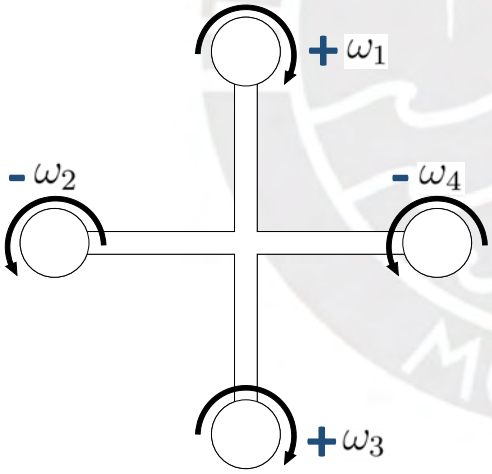

(c) yaw movement

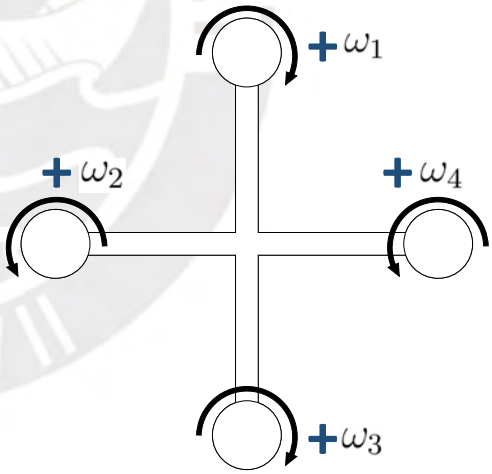

(d) Throttle movement

Figure 2.2: Quadrotor flight movements

2.2. Kinematics

The analysis of kinematics of a rigid body describes the movement of the quadrotor without accounting the external forces that affect itself [69]. For the description of a six degrees of freedom rigid body it is common to designate two reference frames [11] [60]: the inertial frame and the body frame. The inertial frame denoted by {I} is a reference coordinate which is fixed or it moves with uniform velocity; therefore, Newton's laws can be applied [6] [69]. On the other hand, the body frame denoted by {B} is a reference frame which is moving and its coordinates located in the center of gravity of the quadrotor [4].

In the figure below both reference frames can be seen how they are located. The inertial frame also called earth frame is fixed in some point on earth and is described by the X_I, Y_I and Z_I coordinates; therefore, a rigid body can be described by its position [4] [16].

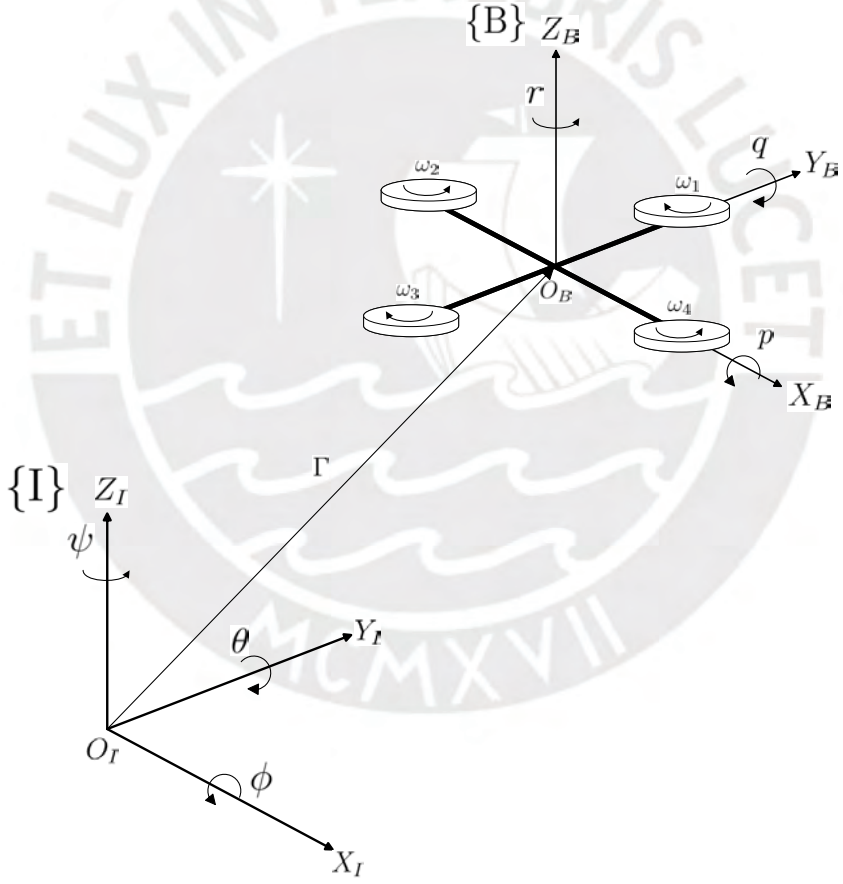

Figure 2.3: Quadrotor's frames setup

The position is defined by the vector:

$$\Gamma = \begin{bmatrix} x_0 & y_0 & z_0 \end{bmatrix} \tag{2.1}$$

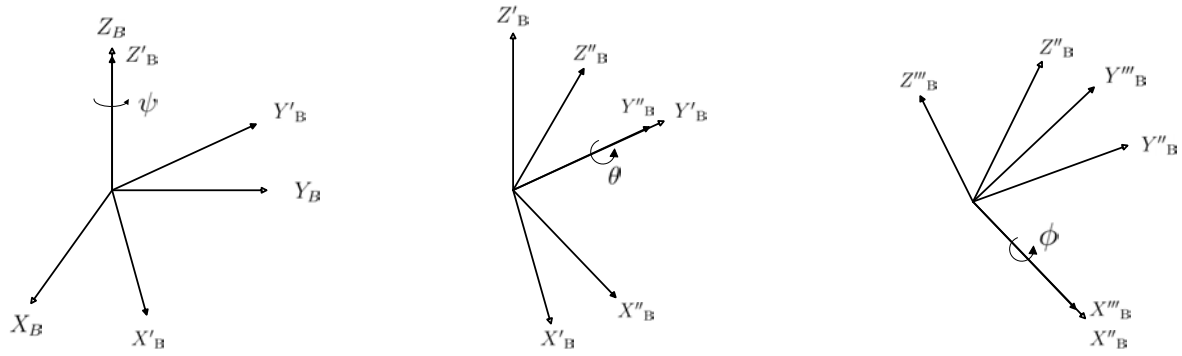

(a) Rotation about Z axis (b) Rotation about Y axis (c) Rotation about X axis

Figure 2.4: Sequence of rotations of the Z-Y-X Euler angles. Based on [15].

The orientation of the quadrotor is defined by three rotations relative to the inertial frame. The rotation angles are the Euler angles: roll, pitch and yaw [69] and they are denoted by the attitude vector.

$$\Omega = \begin{bmatrix} \phi & \theta & \psi \end{bmatrix} \tag{2.2}$$

For describing the aircraft attitude the Z-Y-X Euler rotation is used so information from the body frame to the inertial frame can be obtained. This method consists in rotate about $\mathrm{Z_B}$ axis an angle ψ positive, then rotate about the new Y'_{B} axis an angle θ positive and finally rotate with respect to the new X''_{B} axis an angle ϕ positive [69] [15].

The rotations with respect to the three axis are represented by the following matrices:

Rotation with respect to Z axis:

$$R_Z(\psi) = \begin{bmatrix} cos\psi & -sin\psi & 0 \\ sin\psi & cos\psi & 0 \\ 0 & 0 & 1 \end{bmatrix} \tag{2.3}$$

Rotation with respect to Y axis:

$$R_{Y'}(\theta) = \begin{bmatrix} cos\theta & 0 & sin\theta \\ 0 & 1 & 0 \\ -sin\theta & 0 & cos\theta \end{bmatrix} \tag{2.4}$$

Rotation with respect to X axis:

$$R_{X''}(\phi) = \begin{bmatrix} 1 & 0 & 0 \\ 0 & cos\phi & -sin\phi \\ 0 & sin\phi & cos\phi \end{bmatrix} \tag{2.5}$$

The body frame is changing its position and orientation; therefore, the measurements have to be considered relative to the inertial coordinate system so the mathematical model can be obtained by Newton's laws [6]. By the multiplication of the three rotation matrices:

$${}^{I}_{B}R = \begin{bmatrix} cos\psi & -sin\psi & 0 \\ sin\psi & cos\psi & 0 \\ 0 & 0 & 1 \end{bmatrix} \begin{bmatrix} cos\theta & 0 & sin\theta \\ 0 & 1 & 0 \\ -sin\theta & 0 & cos\theta \end{bmatrix} \begin{bmatrix} 1 & 0 & 0 \\ 0 & cos\phi & -sin\phi \\ 0 & sin\phi & cos\phi \end{bmatrix} \tag{2.6}$$

The relationship between both reference frames is obtained:

$${}^{I}_{B}R(\phi,\theta,\psi) = \begin{bmatrix} cos\theta cos\psi & cos\psi sin\theta sin\phi - cos\phi sin\psi & cos\phi cos\psi sin\theta + sin\phi sin\psi \\ cos\theta sin\psi & sin\theta sin\phi sin\psi + cos\phi cos\psi & cos\phi sin\theta sin\psi - cos\psi sin\phi \\ -sin\theta & cos\theta sin\phi & cos\theta cos\phi \end{bmatrix} \tag{2.7}$$

whereas: $-\frac{\pi}{2} < \phi < \frac{\pi}{2}$, $-\frac{\pi}{2} < \theta < \frac{\pi}{2}$, $-\frac{\pi}{2} < \psi < \frac{\pi}{2}$ to prevent singularities like gimbal lock [4].

${}^{I}_{B}R(\psi,\theta,\phi)$ is the transformation matrix from the body frame to the inertial coordinate system or inertial frame where ϕ, θ and ψ are the Euler angles roll, pitch and yaw, respectively. The inverse matrix ${}^{I}_{B}R^{-1}$ is equal to the transposed ${}^{I}_{B}R^{T}$ and this matrix is the transformation matrix from the fixed coordinate system to the body reference frame ${}^{B}_{I}R(\psi,\theta,\phi)$ [4].

The Euler angular rates $\dot{\Theta}$ are defined in the inertial coordinate system and the angular velocity vector Ω is considered in the body reference frame.

$$\dot{\Theta} = \begin{bmatrix} \dot{\phi} & \dot{\theta} & \dot{\psi} \end{bmatrix}^T \qquad \Omega = \begin{bmatrix} p & q & r \end{bmatrix}^T \tag{2.8}$$

The relationship between those two vectors is the equation below which the transformation

matrix mapping the inertial frame to the body reference frame is denoted [4] [69]:

$$\begin{bmatrix} p \\ q \\ r \end{bmatrix} = \begin{bmatrix} 1 & 0 & -sin\theta \\ 0 & cos\phi & sin\phi cos\theta \\ 0 & -sin\phi & cos\theta cos\phi \end{bmatrix} \begin{bmatrix} \dot{\phi} \\ \dot{\theta} \\ \dot{\psi} \end{bmatrix} \tag{2.9}$$

On the other hand, the inverse transformation which is from the body frame to the inertial frame can be obtained:

$$\begin{bmatrix} \dot{\phi} \\ \dot{\theta} \\ \dot{\psi} \end{bmatrix} = \begin{bmatrix} 1 & sin\phi tan\theta & cos\phi tan\theta \\ 0 & cos\phi & -sin\phi \\ 0 & sin\phi sec\theta & cos\phi sec\theta \end{bmatrix} \begin{bmatrix} p \\ q \\ r \end{bmatrix} \tag{2.10}$$

2.3. Dynamics

For this work the quadrotor is considered a system which has a rigid body so it is assumed that the frame of the aircraft is symmetrical, the propellers are identical and also the four motors which are distributed on the frame symmetrically [32] [58] [15]; therefore, the dynamics for a six degrees of freedom rigid body can be described by the Newton-Euler formalism [4] [60] which expresses the rigid body by translation and rotational or attitude dynamical equations [1].

For the translation dynamics the Newton's second law is used in which the external forces are acting on the quadrotor; that is, in the body frame [30].

$$F = m\dot{V}^B + \Omega \times mV^B \tag{2.11}$$

where F is the vector that represents the external forces applied to the aircraft, m is the mass of the rigid body, V is the translation velocity vector in the body frame, $\dot{V}$ is the acceleration vector in the body frame and Ω is the rotational velocity.

$$F = {}^B_I R F_g + F_M \tag{2.12}$$

where ${}^B_I R$ is the transformation matrix from the inertial reference system to the body coordinate frame, F_g is the gravitational vector and F_M is the vector that is composed of the sum of the forces that are generated by the four motors.

$$F_g = \begin{bmatrix} 0 \\ 0 \\ mg \end{bmatrix} \qquad F_M = \begin{bmatrix} 0 \\ 0 \\ \sum_{i=1}^{4} k\omega_i^2 \end{bmatrix} \tag{2.13}$$

where m is the mass of the quadrotor, g is considered the gravity, k is the thrust coefficient, ω_i is the angular velocity generated by each propeller [3]. Since the equation 2.11 is described in the body reference system, it has to be transformed to the inertial coordinate system multiplying the equation by the transformation matrix ${}^{I}_{B}R$. The centrifugal force $\Omega \times mV^B$ is nullified because of the inertial transformation [44]

$$F_g + {}^{I}_{B}RF_M = m\ddot{\Gamma} \tag{2.14}$$

$$m\begin{bmatrix} \ddot{x} \\ \ddot{y} \\ \ddot{z} \end{bmatrix} = \begin{bmatrix} 0 \\ 0 \\ mg \end{bmatrix} + \begin{bmatrix} cos\theta cos\psi & cos\psi sin\theta sin\phi - cos\phi sin\psi & cos\phi cos\psi sin\theta + sin\phi sin\psi \\ cos\theta sin\psi & sin\theta sin\phi sin\psi + cos\phi cos\psi & cos\phi sin\theta sin\psi - cos\psi sin\phi \\ -sin\theta & cos\theta sin\phi & cos\theta cos\phi \end{bmatrix} \begin{bmatrix} 0 \\ 0 \\ \sum_{i=1}^{4} k\omega_i^2 \end{bmatrix} \tag{2.15}$$

The vector differential equations for the translation dynamics are

$$\begin{bmatrix} \ddot{x} \\ \ddot{y} \\ \ddot{z} \end{bmatrix} = \begin{bmatrix} 0 \\ 0 \\ g \end{bmatrix} + \begin{bmatrix} cos\phi cos\psi sin\theta + sin\phi sin\psi \\ cos\phi sin\theta sin\psi - cos\psi sin\phi \\ cos\theta cos\phi \end{bmatrix} \frac{T}{m} \tag{2.16}$$

Where:

$$T = \sum_{i=1}^{4} k\omega_i^2$$

The rotation motion can be expressed by Euler's equations for rigid body:

$$\tau = I\dot{\Omega} + \Omega \times I\Omega + \tau_{gyro} \tag{2.17}$$

where τ is the external torque vector applied to quadrotor, Ω is the angular velocity vector, $\dot{\Omega}$ is the angular acceleration vector, τ_{gyro} is considered as the gyroscopic effects and I is called the inertia tensor and is noted as a 3x3 matrix [17]:

$$I = \begin{bmatrix} I_x & I_{xy} & I_{xz} \\ I_{yx} & I_y & I_{yz} \\ I_{zx} & I_{zy} & I_z \end{bmatrix} \tag{2.18}$$

The quadrotor is modeled under symmetry assumption about its body frame axis, so the matrix can be simplified as taking the non-diagonal elements by zero values [58]:

$$I = \begin{bmatrix} I_x & 0 & 0 \\ 0 & I_y & 0 \\ 0 & 0 & I_z \end{bmatrix} \tag{2.19}$$

Replacing the vectors and matrices in equation 2.17

$$\begin{bmatrix} \tau_\phi \\ \tau_\theta \\ \tau_\psi \end{bmatrix} = \begin{bmatrix} I_x & 0 & 0 \\ 0 & I_y & 0 \\ 0 & 0 & I_z \end{bmatrix} \begin{bmatrix} \dot{p} \\ \dot{q} \\ \dot{r} \end{bmatrix} + \begin{bmatrix} p \\ q \\ r \end{bmatrix} \times \begin{bmatrix} I_x & 0 & 0 \\ 0 & I_y & 0 \\ 0 & 0 & I_z \end{bmatrix} \begin{bmatrix} p \\ q \\ r \end{bmatrix} + I_r \begin{bmatrix} p \\ q \\ r \end{bmatrix} \times \begin{bmatrix} 0 \\ 0 \\ 1 \end{bmatrix} \omega_r \tag{2.20}$$

where I_r is the total moment of inertia of the propellers and $\omega_r = \omega_1 - \omega_3 + \omega_2 - \omega_4$ is the summation of the angular velocities of the motors, τ_ϕ, τ_θ and τ_ψ are the components of τ corresponding to the torques which produce the roll, pitch and yaw rotations, respectively. In vector form:

$$\begin{bmatrix} \tau_\phi \\ \tau_\theta \\ \tau_\psi \end{bmatrix} = \begin{bmatrix} lk(\omega_4^2 - \omega_2^2) \\ lk(\omega_4^2 - \omega_3^2) \\ d(\omega_1^2 - \omega_2^2 + \omega_3^2 - \omega_4^2) \end{bmatrix} \tag{2.21}$$

where l indicates the distance from the quadrotor's the center of mass to the center of the propeller, k is the thrust coefficient, d stands for the drag coefficient [4] [30]. Multiplying the matrices and vectors the differential attitude dynamic equations of the quadrotor are obtained.

$$\begin{bmatrix} \dot{p} \\ \dot{q} \\ \dot{r} \end{bmatrix} = \begin{bmatrix} \tau_\phi / I_x \\ \tau_\theta / I_y \\ \tau_\psi / I_z \end{bmatrix} + \begin{bmatrix} (I_y - I_z) qr / I_x \\ (I_y - I_z) pr / I_x \\ (I_y - I_z) pq / I_x \end{bmatrix} - I_r \begin{bmatrix} q / I_x \\ -p / I_y \\ 0 \end{bmatrix} \omega_r \tag{2.22}$$

2.4. State space system modelling

The full non linear translational and rotational dynamic equations are represented by equations 2.16 and 2.22. For the state space modeling it is considered without the gyroscopic effects τ_{gyro}. That parameter will be added for the uncertainty analysis. The quadrotor is a multivariable nonlinear system and can be described by the general affine state space form:

$$\dot{x} = f(x) + \sum_{i=1}^{m} g_i(x) u_i \tag{2.23}$$

$$\begin{aligned} y_1 &= h_1(x) \\ &\vdots \\ y_m &= h_m(x) \end{aligned}$$

where $x(t) \in \mathbb{R}^n$, $f(x)$, g_1, $\ldots$ g_m are vector functions. The vector $u = [u_1\ u_2\ \ldots\ u_m]^T$ and the outputs $y = [h_1(x) \quad h_2(x) \quad \ldots \quad h_m(x)]^T$ are smooth nonlinear functions [33] [62]. For the present work, the quadrotor system can be written as:

$$f(x) = \begin{bmatrix} u_0 \\ v_0 \\ w_0 \\ qsin(\phi)sec(\theta) + rcos(\phi)sec(\theta) \\ qcos(\phi) - rsin(\phi) \\ p + qsin(\phi)tan(\theta) + rcos(\phi)tan(\theta) \\ 0 \\ 0 \\ g \\ \frac{I_y - I_z}{I_x} qr \\ \frac{I_z - I_x}{I_y} pr \\ \frac{I_x - I_y}{I_z} pq \end{bmatrix} \tag{2.24}$$

$$g(x) = \begin{bmatrix} 0 & 0 & 0 & 0 \\ 0 & 0 & 0 & 0 \\ 0 & 0 & 0 & 0 \\ 0 & 0 & 0 & 0 \\ 0 & 0 & 0 & 0 \\ 0 & 0 & 0 & 0 \\ -\frac{1}{m}(cos(\phi)cos(\psi)sin(\theta) + sin(\phi)sin(\psi)) & 0 & 0 & 0 \\ -\frac{1}{m}(cos(\phi)sin(\theta)sin(\psi) - cos(\psi)sin(\phi)) & 0 & 0 & 0 \\ -\frac{1}{m}(cos(\theta)cos(\phi) & 0 & 0 & 0 \\ 0 & \frac{1}{I_x} & 0 & 0 \\ 0 & 0 & \frac{1}{I_y} & 0 \\ 0 & 0 & 0 & \frac{1}{I_z} \end{bmatrix} \tag{2.25}$$

The state vector is as follows:

$$x = \begin{bmatrix} x_0 & y_0 & z_0 & \psi & \theta & \phi & u_0 & v_0 & w_0 & p & q & r \end{bmatrix}^T \tag{2.26}$$

The control law is a 4x1 vector:

$$u = \begin{bmatrix} u_1 & u_2 & u_3 & u_4 \end{bmatrix}^T \tag{2.27}$$

where u_1 is the combined thrust produced by the four motors, u_2, u_3 and u_4 represent the roll, pitch and yaw torques, respectively.

For the output vector it is proposed to control the position and the yaw angle variables:

$$y = \begin{bmatrix} x_0 \\ y_0 \\ z_0 \\ \psi \end{bmatrix} \tag{2.28}$$

Then the vector is represented by twelve state space variables:

$$x = \begin{bmatrix} x_1 & x_2 & x_3 & x_4 & x_5 & x_6 & x_7 & x_8 & x_9 & x_{10} & x_{11} & x_{12} \end{bmatrix}^T \tag{2.29}$$

Replacing the state space variables in $f(x)$ and $g(x)$:

$$f(x) = \begin{bmatrix} x_7 \\ x_8 \\ x_9 \\ x_{11}sin(x_6)sec(x_5) + x_{12}cos(x_6)sec(x_5) \\ x_{11}cos(x_6) - x_{12}sin(x_6) \\ x_{10} + x_{11}sin(x_6)tan(x_5) + x_{12}cos(x_6)tan(x_5) \\ 0 \\ 0 \\ g \\ \frac{I_y - I_z}{I_x} x_{11}x_{12} \\ \frac{I_z - I_x}{I_y} x_{10}x_{12} \\ \frac{I_x - I_y}{I_z} x_{10}x_{11} \end{bmatrix} \tag{2.30}$$

$$g(x) = \begin{bmatrix} 0 & 0 & 0 & 0 \\ 0 & 0 & 0 & 0 \\ 0 & 0 & 0 & 0 \\ 0 & 0 & 0 & 0 \\ 0 & 0 & 0 & 0 \\ 0 & 0 & 0 & 0 \\ -\frac{1}{m}(cos(x_6)cos(x_4)sin(x_5) + sin(x_6)sin(x_4)) & 0 & 0 & 0 \\ -\frac{1}{m}(cos(x_6)sin(x_5)sin(x_4) - cos(x_4)sin(x_6)) & 0 & 0 & 0 \\ -\frac{1}{m}(cos(x_5)cos(x_6) & 0 & 0 & 0 \\ 0 & \frac{1}{I_x} & 0 & 0 \\ 0 & 0 & \frac{1}{I_y} & 0 \\ 0 & 0 & 0 & \frac{1}{I_z} \end{bmatrix} \tag{2.31}$$

In this subsection the mathematical description of the quadrotor system was presented. The system is composed by six differential dynamical equations that indicate translational and rotational movements. This refers to the concept of six degrees of freedom (6 DOF) of a rigid body. Therefore, in the sense of the quadrotor movements it means that the aircraft can move forward/backward, left/right, up/down along the x, y, z position axes, respectively and rotate around the roll, pitch and yaw axes, respectively. Then, affine state space representation expressed the dynamics of the system, twelve state variables, four inputs (thrust, roll, pitch and yaw torques) and four outputs (position and yaw rotation angle) were selected for the MIMO (Multi-Input Multi-Output) analysis and control design.

Chapter 3

Control Design

3.1. Model Following Control

In this Chapter a model following controller for a nonlinear six degrees of freedom Multi-Input Multi-Output (MIMO) quadrotor system is proposed for the design. This strategy is a two-degree-of-freedom control structure consisting in two loops: first, a nominal controller is designed which is based on the process model in a Model Control Loop(MCL). Then, a second controller acting on the physical process is designed. This is called a Process Control Loop (PCL) which relies on the error dynamics between the model and the actual process states. The architecture of the control strategy is the one used in [75] and the block diagram is presented in Figure 3.1.

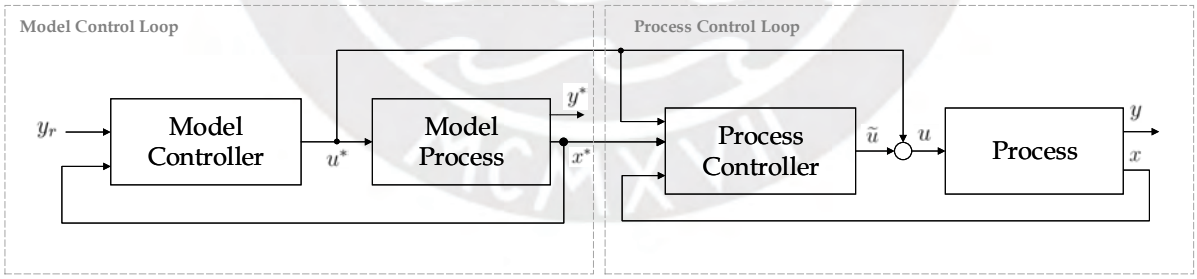

Figure 3.1: Block diagram of the model following control scheme. Based on [75].

where y_r is the reference signal. u^* and y^* are the control input and the output signal, respectively and x^* represents the states of the ideal process. In the process control loop, the reference is the considered states x^* of the model, x and y are the states and the output of the process and $u = u^* + \tilde{u}$ is the control law. The task is to track the reference signal y_r asymptotically.

The nonlinear system is considered as multivariable Byrnes-Isidori-form.

$$\dot{\eta} = f_0(\eta, \xi) \tag{3.1}$$

$$\begin{aligned}
\dot{\xi}_1^i &= \dot{\xi}_2^i \\
&\vdots \\
\dot{\xi}_{r_i-1}^i &= \xi_{r_i}^i \\
\dot{\xi}_{r_i}^i &= a_i(\xi, \eta) + \sum_{j=1}^{m} b_{ij}(\xi, \eta) u_j + \Psi_i(\xi) \\
y_i &= \xi_1^i
\end{aligned}$$

where $\dot{\eta} \in \mathbb{R}^{n-r}$ and $\dot{\xi} \in \mathbb{R}^r$ represent the internal and external dynamics, respectively. $y_i \in \mathbb{R}^m$ and $u_i \in \mathbb{R}^m$ are the output and the input of the system, respectively; with the unknown model uncertainty $\Psi_i(\xi)$.

$$\begin{aligned}
a_i(\xi, \eta) &= L_f^{r_i} h_i(\Phi^{-1}(\xi, \eta)) \\
b_{ij}(\xi, \eta) &= L_{g_j} L_f^{r_i - 1} h_i(\Phi^{-1}(\xi, \eta))
\end{aligned}$$

For $1 \leq i \leq m$, $1 \leq j \leq m$

$\Phi(\xi, \eta)$ is a local coordinate vector transformation in a neighborhood of x_δ where $L_{g_j} L_f^{r_i - 1} h_i(x_\delta) \neq 0$ [33]. The expression $L_f h_1(x)$ is the Lie derivative that means the rate of change of $h(x)$ along the smooth vector field $f(x) = [f_1(x), f_2(x) ... f_n(x)]^T$ at the point x which is define as [42] [57] [54]:

$$L_f h_i(x) = \sum_{j=1}^{n} \frac{\partial h_i}{\partial x_j} f_j(x)$$

In a recursive expression

$$L_f^k h_i(x) = \sum_{j=1}^{n} \frac{\partial L_f^{k-1} h_i(x)}{\partial x_j} f_j(x)$$

A vector relative degree is defined for the system $r = \{r_1, r_2, r_3, ..., r_i\}$ where r_i is the relative degree with respect to the ith output and it is defined as how many times the ith output has

to be differentiated so that at least one of the m inputs of the system appears in the output equation ith [61].

For the control law design exact feedback linearization is applied for the model control loop (MCL) and the process control loop (PCL) based on the nonlinear model. Feedback linearization technique is used in this work due to its principle of canceling the nonlinearity of the process [51]. In this work it is considered the special case of dynamic extension for MIMO systems to get the decoupling matrix nonsingular and achieve full relative degree [33]. Furthermore, high gain control technique is developed in the process control loop (PCL) to enhance the robustness in the feedback system so the model uncertainties can be compensated [76]. Additional investigation on linear and nonlinear systems with high-gain state feedback controllers are obtained in [13] [23]. For robustness performance, uncertainty analysis is developed for the complete system.

3.1.1. Feedback Linearization

Feedback linearization is a nonlinear control strategy that converts a nonlinear dynamics into a corresponding linear one by canceling the nonlinearities of the system so the designer can apply linear control techniques [73] [63]. In this section a feedback control law is designed with feedback linearization technique for a Multi-Input Multi-Output (MIMO) quadrotor system applying a coordinate transformation in state-space to obtain a linear model. This is called exact linearization and the goal is to solve the input-output decoupling problem in order to obtain the system decomposed into single-input single-output subsystems. [33]

Considering the MIMO system in equation 2.23 it is defined the vector relative degree $r = \{r_1, r_2, r_3, ..., r_i\}$ where r_i is the relative degree with respect to the ith output. The relative degree of the system is defined at the point $x = x_0$ if it fulfills the conditions[33]:

i) For all x values in a open neighborhood of x_δ

$$L_{g_j} L_f^k h_i(x) = 0$$

For all $1 \leq i \leq m$, for all $1 \leq j \leq m$, for all $k < r_i - 1$

ii) The decoupling matrix $m \times m$

$$b(x) = \begin{bmatrix} L_{g_1} L_f^{r_1 - 1} h_1(x) & ... & L_{g_m} L_f^{r_1 - 1} h_1(x) \\ \vdots & \ddots & \vdots \\ L_{g_1} L_f^{r_m - 1} h_m(x) & ... & L_{g_m} L_f^{r_m - 1} h_m(x) \end{bmatrix}$$

is invertible or nonsingular in the point $x = x_\delta$.

Consequently, the following relation is derived:

$$\begin{bmatrix} y_1^{(r_1)} \\ \vdots \\ y_4^{(r_m)} \end{bmatrix} = a(x) + b(x)u$$

where:

$$a(x) = \begin{bmatrix} L_f^{r_1} h_1(x) \\ \vdots \\ L_f^{r_m} h_m(x) \end{bmatrix}$$

Based on the definition of relative degree vector and the matrix $b(x)$ invertible, therefore the state feedback control law is defined:

$$u = \alpha(x) + \beta(x)v \tag{3.2}$$

where:

$$\alpha(x) = -b(x)^{-1}a(x)$$
$$\beta(x) = b(x)^{-1}$$
$$v = [v_1 \ v_2 \ ... \ v_m]^T$$

In Figure 3.2 it is shown a block diagram of the feedback linearization algorithm implemented for a nonlinear system. The state feedback control law transform the nonlinear system into an input-output decoupling relationship that results in the closed-loop system:

$$\begin{bmatrix} y_1^{(r_1)} \\ \vdots \\ y_4^{(r_m)} \end{bmatrix} = \begin{bmatrix} v_1 \\ \vdots \\ v_m \end{bmatrix}$$

For all $1 \leq i \leq m$ and $v = [v_1 \ v_2 \ ... \ v_m]^T$ is the linear control vector.

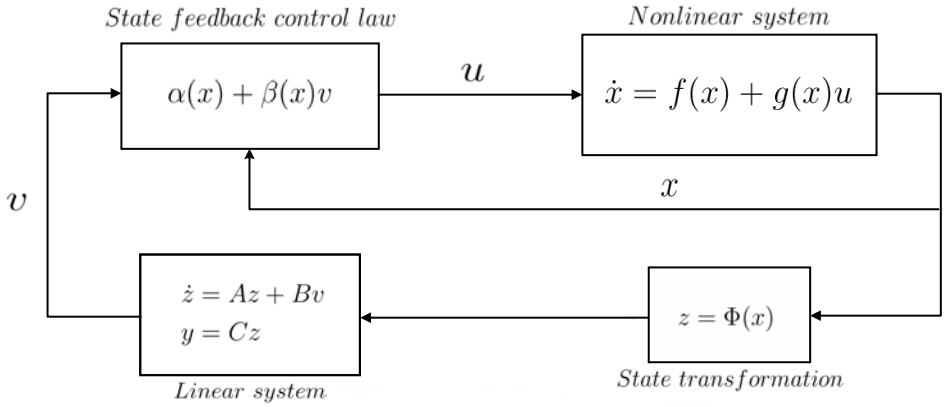

Figure 3.2: Feedback linearization block diagram applied to nonlinear system.

Consider the total relative degree for the MIMO system of equation 2.23 in the following statement [26]:

$$r = r_1 + r_2 + ... + r_m \leq n$$

Therefore, the nonlinear process can be transformed by a change of variables $z = \Phi(x)$ where z, the new state, is composed by a vector ξ with dimension m and a vector η with dimension $n - r$ that depends on the variables ξ and η and which fulfills a differential equation [36] [33]. This statement is shown in the next case:

If $r < n$, transformation state variables stays:

$$z = \Phi(x) = \begin{bmatrix} \phi_1^1(x) \\ \vdots \\ \phi_{r_1}^1(x) \\ \vdots \\ \phi_1^m(x) \\ \vdots \\ \phi_{r_m}^m(x) \\ \phi_{r+1}(x) \\ \vdots \\ \phi_n(x) \end{bmatrix}$$

The terms $\phi_{r+1}(x)$, ... , $\phi_n(x)$ which are continuous differential functions are chosen in a manner that

$$L_{g_j}\phi_i(x) = \frac{\partial \phi_i(x)}{\partial x} g_j(x) = 0 \tag{3.3}$$

For $r+1 \leq i \leq n$, for $1 \leq j \leq m$ and $\forall\ x$ near the neighborhood of x_δ

To ensure the expression above in 3.3 the generated spanned distribution of the vector fields $g_1(x)$, ... , $g_m(x)$ should be involutive and that implies solving partial differential equations for $\phi_{r+1}(x)$, ... , $\phi_n(x)$ [41].

Therefore, the change of variables is divided into the set:

$$\xi^i = \begin{bmatrix} \xi_1^i \\ \xi_2^i \\ \vdots \\ \xi_{r_i}^i \end{bmatrix} = \begin{bmatrix} \phi_1^i(x) \\ \phi_2^i(x) \\ \vdots \\ \phi_{r_i}^i(x) \end{bmatrix}$$

$$\xi = \begin{bmatrix} \xi^1 & \xi^2 & \dots & \xi^m \end{bmatrix}$$

$$\eta = \begin{bmatrix} \eta_1 \\ \eta_2 \\ \vdots \\ \eta_{n-r} \end{bmatrix} = \begin{bmatrix} \phi_{r+1} \\ \phi_{r+2} \\ \vdots \\ \phi_{n-r} \end{bmatrix}$$

Then the dynamic equations obtained are found in 3.1 .

If $r = n$, that means the sum of the elements for the vector relative degree correspond to the number of states and the variable η is not considered in the transformation of coordinates states, then the transformation variables is obtained as:

$$\xi^i = \begin{bmatrix} y_1^{(r_1)} \\ \vdots \\ y_4^{(r_m)} \end{bmatrix} = \begin{bmatrix} \dot{\xi}_1^i \\ \dot{\xi}_2^i \\ \vdots \\ \dot{\xi}_{r_i}^i \end{bmatrix} = \begin{bmatrix} \phi_1^i(x) \\ \phi_2^i(x) \\ \vdots \\ \phi_{r_i}^i(x) \end{bmatrix} = \begin{bmatrix} h_i(x) \\ L_f h_i(x) \\ \vdots \\ L_f^{r_i-1} h_i(x) \end{bmatrix}$$

For $1 \leq i \leq m$

Then, the relative degree of the output h_i of the nonlinear system is r_i. For the first output of the system that corresponds the position in x axis:

$$h_1(x) = x_0$$

The first Lie derivative is obtained:

$$\begin{aligned} L_f h_1(x) &= \frac{\partial h_1(x)}{\partial x}(f(x) + g(x)u) \\ &= u_0 \end{aligned}$$

which is the velocity in x axis.

Then, the second Lie derivative is obtained:

$$\begin{aligned} L_f^2 h_1(x) &= \frac{\partial L_f h_1(x)}{\partial x}(f(x) + g(x)u) \\ &= -\frac{1}{m}(sin(x_4)sin(x_6) + cos(x_4)cos(x_6)sin(x_5))u_1 \end{aligned}$$

So the control law u_1 affects the system through the second derivative of $h_1(x)$ which indicates that the relative degree related to the first output is $r_1 = 2$. The same procedure is applied to the other output components y_0, z_0 and ψ.

For $h_2(x) = y_0$, the input u_1 appears in the second Lie derivative:

$$\begin{aligned} L_f^2 h_2(x) &= \frac{\partial L_f h_2(x)}{\partial x}(f(x) + g(x)u) \\ &= -\frac{1}{m}(cos(x_6)sin(x_5)sin(x_4) - cos(x_4)sin(x_6))u_1 \end{aligned}$$

For $h_3(x) = z_0$, the input u_1 also appears in the second Lie derivative:

$$\begin{aligned} L_f^2 h_3(x) &= \frac{\partial L_f h_3(x)}{\partial x}(f(x) + g(x)u) \\ &= g - \frac{1}{m}(cos(x_5)cos(x_6))u_1 \end{aligned}$$

and the first and second Lie derivative for the output $h_4(x) = \psi$:

$$\begin{aligned} L_f h_4(x) &= \frac{\partial L_f h_4(x)}{\partial x}(f(x) + g(x)u) \\ &= x_{13}sin(x_6)sec(x_5) + x_{14}cos(x_6)sec(x_5) \end{aligned}$$

$$\begin{aligned} L_f^2 h_4(x) &= \frac{\partial L_f h_4(x)}{\partial x}(f(x) + g(x)u) \\ &= \frac{\partial L_f h_4(x)}{\partial x}(f(x)) + \frac{1}{I_y}sin(x_6)sec(x_5)u_3 + \frac{1}{I_z}cos(x_6)sec(x_5)u_4 \end{aligned}$$

The term $\frac{\partial L_f h_4(x)}{\partial x}(f(x))$ was indicated as mathematical expression due to the inputs appeared multiplying just the term $g(x)$. Therefore, for the nonlinear system in 2.23 the elements of the vector relative degree are:

$$r_1 = r_2 = r_3 = r_4 = 2$$

And the total relative degree of the system

$$r_1 + r_2 + r_3 + r_4 = 8$$

is less than the number of states $n = 12$. Then, new coordinates η and ξ could be found; nevertheless, the decoupling matrix must be analyzed:

$$b(x) = \begin{bmatrix} -\frac{sin(x_4)sin(x_6)+cos(x_4)cos(x_6)sin(x_5)}{m} & 0 & 0 & 0 \\ \frac{cos(x_4)sin(x_6)-cos(x_6)sin(x_4)sin(x_5)}{m} & 0 & 0 & 0 \\ -\frac{cos(x_5),cos(x_6)}{m} & 0 & 0 & 0 \\ 0 & 0 & \frac{sin(x_6)}{Iy,cos(x_5)} & \frac{cos(x_6)}{Iz,cos(x_5)} \end{bmatrix}$$

For the values of x_i the matrix $b(x)$ is singular or non-invertible. This is proven by obtaining the determinant:

$$det(b(x)) = 0$$

Therefore, the problem of input-output for the nonlinear system 2.23 can not be solved and a state feedback control law can not be designed. It is shown that the control law u_1 influences the second Lie derivative of $h_1(x)$, $h_2(x)$ and $h_3(x)$. In the next subsection it is presented the concept of dynamic extension that demonstrate the achievement of the total relative degree by adding more states variables to the system, then a dynamic feedback control law can be designed.

Feedback linearization is a technique for linearizing nonlinear systems. It was applied to the quadrotor system to obtain an independent single input single output subsystems. It was shown that it could not be done since the matrix $b(x)$ was singular; hence, the concept of dynamic extension is applied in the next section. This notion will allow to achieve the relative degree and obtain the inverse of the decoupling matrix. Therefore, the input-output decoupling problem is solved.

3.2. Feedback linearization with dynamic extension

In the last section input u_1 appeared in the second Lie derivative with respect to the outputs $h_1(x)$, $h_2(x)$ and $h_3(x)$. This caused to have a singular matrix; therefore, the input-output decoupling problem could not be solved. The next procedure will cause the input u_1 delay its appearance in the Lie derivative expression for higher order derivatives. So in this section additional states are considered in the system. The technique called dynamic state feedback is applied in order to achieve the total relative degree of the MIMO nonlinear system [33]. This type of feedback can be mathematically described using the equations of the form:

where the control input u becomes a new state for dynamical system and $\dot{\zeta}$ is a new dynamic feedback, v is an external reference input and y stays the same output of the system. In this procedure the input u_1 will be equal to a dynamics system in order to delay its appearance in

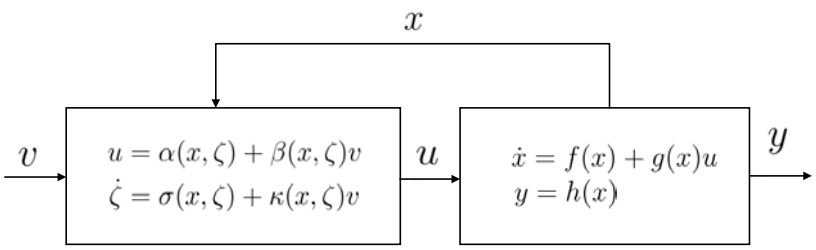

Figure 3.3: Configuration of the augmented system. Based on [33].

the Lie derivative with respect to the three first outputs. The technique applied for this work in considered according to [33]. First the output u_1 is taken as the output of an integrator. This is shown in the new equation

$$\begin{aligned} u_1 &= \zeta \\ \dot{\zeta} &= \overline{u}_1 \end{aligned}$$

where u_1 is the new state as ζ and $\overline{u}_1$ is considered as a virtual input that then have to be integrated to obtain the real control input for the dynamical system. The new system is composed by thirteen state variables and can be shown in the new state space vector

$$x = \begin{bmatrix} x_0 & y_0 & z_0 & \psi & \theta & \phi & u_0 & v_0 & w_0 & \zeta & p & q & r \end{bmatrix}^T \tag{3.4}$$

The function component $f(x)$ of the nonlinear system has increased its components and stays as

$$f(x) = \begin{bmatrix} x_7 \\ x_8 \\ x_9 \\ x_{13}cos(x_6)sec(x_5) + x_{12}sin(x_6)sec(x_5) \\ x_{12}\ \cos(x_6) - x_{13}\ \sin(x_6) \\ x_{11} + x_{13}cos(x_6)tan(x_5) + x_{12}sin(x_6)tan(x_5) \\ -\frac{x_{10}}{m}(sin(x_4)sin(x_6) + cos(x_4)cos(x_6)sin(x_5)) \\ \frac{x_{10}}{m}(cos(x_4)sin(x_6) - cos(x_6)sin(x_4)sin(x_5)) \\ g - x_{10}\ \cos(x_5)\ \cos(x_6) \\ 0 \\ \frac{I_y - I_z}{I_x}x_{12}x_{13} \\ \frac{I_z - I_x}{I_y}x_{11}x_{13} \\ \frac{I_x - I_y}{I_z}x_{11}x_{12} \end{bmatrix} \tag{3.5}$$

The components of the vector relative degree of the nonlinear system with one state variable integrated:

$$\begin{aligned} r_1 = r_2 = r_3 = 3 \\ r_4 = 2 \end{aligned}$$

And the total relative degree is

$$r_1 + r_2 + r_3 + r_4 = 11$$

and the calculation of the decoupling matrix $b(x)$:

$$b(x) = \begin{bmatrix} -\frac{\sin(x_6)\sin(x_4)+\sin(x_5)\cos(x_4)\cos(x_6)}{m} & -\frac{x_{10}\,(\sin(x_4)\cos(x_6)-\cos(x_4)\sin(x_5)\sin(x_6))}{\mathrm{Ix}\,m} & -\frac{x_{10}\cos(x_5)\cos(x_4)}{\mathrm{Iy}\,m} & 0 \\ \frac{\cos(x_4)\sin(x_6)-\cos(x_6)\sin(x_5)\sin(x_4)}{m} & \frac{x_{10}\,(\cos(x_4)\cos(x_6)+\sin(x_4)\sin(x_5)\sin(x_6))}{\mathrm{Ix}\,m} & -\frac{x_{10}\cos(x_5)\sin(x_4)}{\mathrm{Iy}\,m} & 0 \\ -\frac{\cos(x_6)\cos(x_5)}{m} & \frac{x_{10}\cos(x_5)\sin(x_6)}{\mathrm{Ix}\,m} & \frac{x_{10}\sin(x_5)}{\mathrm{Iy}\,m} & 0 \\ 0 & 0 & \frac{\sin(x_6)}{\mathrm{Iy}\cos(x_5)} & \frac{\cos(x_6)}{\mathrm{Iz}\cos(x_5)} \end{bmatrix}$$

The determinant of the decoupling matrix is calculated

$$det(b(x)) = 0$$

This means that the matrix is singular or non-invertible because the value is zero so the problem of input-output decoupling can not be solved again. Therefore, a second integrator is added to the system

In this case the addition of two virtual state variables are considered to the nonlinear dynamical system. The input u_1 now is the output of a double integrator in chain form:

$$\begin{aligned} u_1 &= \zeta \\ \dot{\zeta} &= \xi \\ \dot{\xi} &= \overline{u}_1 \end{aligned}$$

The state space vector now has fourteen variables:

$$x = \begin{bmatrix} x_0 & y_0 & z_0 & \psi & \theta & \phi & u_0 & v_0 & w_0 & \zeta & \xi & p & q & r \end{bmatrix}^T \tag{3.6}$$

$$x = \begin{bmatrix} x_1 & x_2 & x_3 & x_4 & x_5 & x_6 & x_7 & x_8 & x_9 & x_{10} & x_{11} & x_{12} & x_{13} & x_{14} \end{bmatrix}^T$$

and the augmented state space differential equation has the following form

$$f(x) = \begin{bmatrix} x_7 \\ x_8 \\ x_9 \\ x_{13}sin(x_6)sec(x_5) + x_{14}cos(x_6)sec(x_5) \\ x_{13}cos(x_6) - x_{14}sin(x_6) \\ x_{12} + x_{13}sin(x_6)tan(x_5) + x_{14}cos(x_6)tan(x_5) \\ -\frac{x_{10}}{m}(sin(x_4)sin(x_6) + cos(x_4)cos(x_6)sin(x_5)) \\ \frac{x_{10}}{m}(cos(x_4)sin(x_6) - cos(x_6)sin(x_4)sin(x_5)) \\ g - x_{10}\ \cos(x_5)\ \cos(x_6) \\ x_{11} \\ 0 \\ \frac{I_y - I_z}{I_x}x_{13}x_{14} \\ \frac{I_z - I_x}{I_y}x_{12}x_{14} \\ \frac{I_x - I_y}{I_z}x_{12}x_{13} \end{bmatrix} \tag{3.7}$$

$$g(x) = \begin{bmatrix} 0 & 0 & 0 & 0 \\ 0 & 0 & 0 & 0 \\ 0 & 0 & 0 & 0 \\ 0 & 0 & 0 & 0 \\ 0 & 0 & 0 & 0 \\ 0 & 0 & 0 & 0 \\ 0 & 0 & 0 & 0 \\ 0 & 0 & 0 & 0 \\ 0 & 0 & 0 & 0 \\ 1 & 0 & 0 & 0 \\ 0 & \frac{1}{I_x} & 0 & 0 \\ 0 & 0 & \frac{1}{I_y} & 0 \\ 0 & 0 & 0 & \frac{1}{I_z} \end{bmatrix} \tag{3.8}$$

The total relative degree fo the system is

$$\begin{aligned} r_1 = r_2 = r_3 = 4 \\ r_4 = 2 \\ r_1 + r_2 + r_3 + r_4 = 14 \end{aligned}$$

For the outputs $h_1(x) = x_0$, $h_2(x) = y_0$, $h_3(x) = z_0$ the relative degree is four due to the appearance of the control inputs in the fourth derivative and for the output $h_4(x) = \psi$ the relative degree stays at two. And the decoupling matrix is shown:

$$b(x) = \begin{bmatrix} -\frac{\sin(x_4)\sin(x_6)+\cos(x_4)\cos(x_6)\sin(x_5)}{m} & -\frac{x_{10}\left(\cos(x_6)\sin(x_4)-\cos(x_4)\sin(x_5)\sin(x_6)\right)}{\mathrm{Ix}\,m} & -\frac{x_{10}\cos(x_4)\cos(x_5)}{\mathrm{Iy}\,m} & 0 \\ \frac{\cos(x_4)\sin(x_6)-\cos(x_6)\sin(x_4)\sin(x_5)}{m} & \frac{x_{10}\left(\cos(x_4)\cos(x_6)+\sin(x_4)\sin(x_5)\sin(x_6)\right)}{\mathrm{Ix}\,m} & -\frac{x_{10}\cos(x_5)\sin(x_4)}{\mathrm{Iy}\,m} & 0 \\ -\frac{\cos(x_5)\cos(x_6)}{m} & \frac{x_{10}\cos(x_5)\sin(x_6)}{\mathrm{Ix}\,m} & \frac{x_{10}\sin(x_5)}{\mathrm{Iy}\,m} & 0 \\ 0 & 0 & \frac{\sin(x_6)}{\mathrm{Iy}\cos(x_5)} & \frac{\cos(x_6)}{\mathrm{Iz}\cos(x_5)} \end{bmatrix}$$

is non-singular or invertible since the determinant has nonzero value [70]:

$$det(b(x)) = -\frac{{x_{10}}^2 \cos(x_6)}{\mathrm{Ix}\,\mathrm{Iy}\,\mathrm{Iz}\,m^3 \cos(x_5)}$$

Then, the problem of decoupling the input and output of the system in equation 2.23 can be solved by applying the dynamic control law:

$$u = \alpha(x, \zeta, \xi) + \beta(x, \zeta, \xi)v \tag{3.9}$$

The expression has a similar structure to the equation 3.2 considering the additional internal state variables ξ and ζ. The structure of the dynamic extension applied to the nonlinear system is shown in Figure 3.4

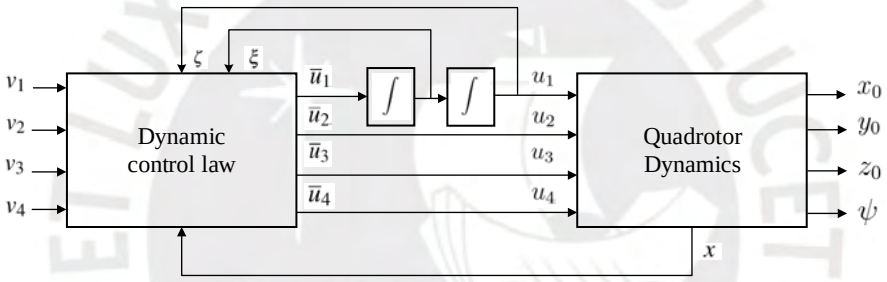

Figure 3.4: The system with two additional states. Based on [47].

The original control inputs u_1, u_2, u_3 and u_4 were substituted by $\overline{u}_1$, $\overline{u}_2$, $\overline{u}_3$ and $\overline{u}_4$ respectively. A delay of two integrators was applied to the control input u_1 obtaining two internal state variables while the other control inputs have no modifications.

The mapping of the local coordinate vector transformation is given by:

$$z = \begin{bmatrix} h_1(x) \\ L_f h_1(x) \\ L_f^2 h_1(x) \\ L_f^3 h_1(x) \\ h_2(x) \\ L_f h_2(x) \\ L_f^2 h_2(x) \\ L_f^3 h_2(x) \\ h_3(x) \\ L_f h_3(x) \\ L_f^2 h_3(x) \\ L_f^3 h_3(x) \\ h_4(x) \\ L_f h_4(x) \end{bmatrix} = \begin{bmatrix} x_1 \\ x_7 \\ -\frac{x_{10}\,\sigma_3}{m} \\ -\frac{x_{11}\,\sigma_3}{m} - \frac{x_{10}\,(\sin(x_4)\cos(x_6) - \cos(x_4)\sin(x_6)\sin(x_5))\,\sigma_4}{m} - \frac{x_{10}\,\sigma_1\,\sigma_2}{m} - \frac{x_{10}\cos(x_5)\cos(x_4)\cos(x_6)\,\sigma_5}{m} \\ x_2 \\ x_8 \\ \frac{x_{10}\,\sigma_2}{m} \\ \frac{x_{11}\,\sigma_2}{m} + \frac{x_{10}\,(\cos(x_6)\cos(x_4) + \sin(x_6)\sin(x_5)\sin(x_4))\,\sigma_4}{m} - \frac{x_{10}\,\sigma_1\,\sigma_3}{m} - \frac{x_{10}\cos(x_5)\cos(x_6)\sin(x_4)\,\sigma_5}{m} \\ x_3 \\ x_9 \\ g - \frac{x_{10}\cos(x_5)\cos(x_6)}{m} \\ \frac{x_{10}\cos(x_6)\sin(x_5)\,\sigma_5}{m} - \frac{x_{11}\cos(x_5)\cos(x_6)}{m} + \frac{x_{10}\cos(x_5)\sin(x_6)\,\sigma_4}{m} \\ x_4 \\ \sigma_1 \end{bmatrix} \tag{3.10}$$

where

$\sigma_1 = \frac{x_{14}\cos(x_6)}{\cos(x_5)} + \frac{x_{13}\sin(x_6)}{\cos(x_5)}$

$\sigma_2 = \cos(x_4)\,\sin(x_6) - \cos(x_6)\,\sin(x_4)\,\sin(x_5)$

$\sigma_3 = \sin(x_4)\,\sin(x_6) + \cos(x_4)\,\cos(x_6)\,\sin(x_5)$

$\sigma_4 = x_{12} + x_{14}\cos(x_6)\,\tan(x_5) + x_{13}\sin(x_6)\,\tan(x_5)$

$\sigma_5 = x_{13}\cos(x_6) - x_{14}\sin(x_6)$

Differentiating with respect to time the new coordinate system, exhibits the following state-space representation.

$$\begin{aligned} \dot{z} &= Az + Bv \\ y &= Cz \end{aligned} \tag{3.11}$$

The states of the new coordinate linear system:

$$z = \begin{bmatrix} z_1 & z_2 & z_3 & z_4 & z_5 & z_6 & z_7 & z_8 & z_9 & z_{10} & z_{11} & z_{12} & z_{13} & z_{14} \end{bmatrix}^T$$

where A denotes the system matrix, B represents the input matrix, and C the output matrix. The corresponding values for the linear system are

$$A = \begin{bmatrix} 0 & 1 & 0 & 0 & 0 & 0 & 0 & 0 & 0 & 0 & 0 & 0 & 0 & 0 \\ 0 & 0 & 1 & 0 & 0 & 0 & 0 & 0 & 0 & 0 & 0 & 0 & 0 & 0 \\ 0 & 0 & 0 & 1 & 0 & 0 & 0 & 0 & 0 & 0 & 0 & 0 & 0 & 0 \\ 0 & 0 & 0 & 0 & 0 & 0 & 0 & 0 & 0 & 0 & 0 & 0 & 0 & 0 \\ 0 & 0 & 0 & 0 & 0 & 1 & 0 & 0 & 0 & 0 & 0 & 0 & 0 & 0 \\ 0 & 0 & 0 & 0 & 0 & 0 & 1 & 0 & 0 & 0 & 0 & 0 & 0 & 0 \\ 0 & 0 & 0 & 0 & 0 & 0 & 0 & 1 & 0 & 0 & 0 & 0 & 0 & 0 \\ 0 & 0 & 0 & 0 & 0 & 0 & 0 & 0 & 0 & 0 & 0 & 0 & 0 & 0 \\ 0 & 0 & 0 & 0 & 0 & 0 & 0 & 0 & 0 & 1 & 0 & 0 & 0 & 0 \\ 0 & 0 & 0 & 0 & 0 & 0 & 0 & 0 & 0 & 0 & 1 & 0 & 0 & 0 \\ 0 & 0 & 0 & 0 & 0 & 0 & 0 & 0 & 0 & 0 & 0 & 1 & 0 & 0 \\ 0 & 0 & 0 & 0 & 0 & 0 & 0 & 0 & 0 & 0 & 0 & 0 & 0 & 0 \\ 0 & 0 & 0 & 0 & 0 & 0 & 0 & 0 & 0 & 0 & 0 & 0 & 0 & 1 \\ 0 & 0 & 0 & 0 & 0 & 0 & 0 & 0 & 0 & 0 & 0 & 0 & 0 & 0 \end{bmatrix} \tag{3.12}$$

$$B = \begin{bmatrix} 0 & 0 & 0 & 0 \\ 0 & 0 & 0 & 0 \\ 0 & 0 & 0 & 0 \\ 1 & 0 & 0 & 0 \\ 0 & 0 & 0 & 0 \\ 0 & 0 & 0 & 0 \\ 0 & 0 & 0 & 0 \\ 0 & 1 & 0 & 0 \\ 0 & 0 & 0 & 0 \\ 0 & 0 & 0 & 0 \\ 0 & 0 & 0 & 0 \\ 0 & 0 & 1 & 0 \\ 0 & 0 & 0 & 0 \\ 0 & 0 & 0 & 1 \end{bmatrix} \tag{3.13}$$

$$C = \begin{bmatrix} 1 & 0 & 0 & 0 & 0 & 0 & 0 & 0 & 0 & 0 & 0 & 0 & 0 & 0 \\ 0 & 0 & 0 & 0 & 1 & 0 & 0 & 0 & 0 & 0 & 0 & 0 & 0 & 0 \\ 0 & 0 & 0 & 0 & 0 & 0 & 0 & 0 & 1 & 0 & 0 & 0 & 0 & 0 \\ 0 & 0 & 0 & 0 & 0 & 0 & 0 & 0 & 0 & 0 & 0 & 0 & 1 & 0 \end{bmatrix} \tag{3.14}$$

The linear control inputs are :

$$v = \begin{bmatrix} v_1 \\ v_2 \\ v_3 \\ v_4 \end{bmatrix}$$

The C matrix shows that the outputs of the linear system are the same of the nonlinear original one.

After the linearization of a nonlinear system, linear control techniques can be applied. For this model; for instance, Proportional-Integral-Derivative (PID) Control, pole placement or linear quadratic regulator (LQR) can be designed.

3.3. Model Control Loop

In the Model Control Loop a feedback linearization controller is developed for the nominal quadrotor's mathematical model. The nominal model considers the mathematical equations of the aircraft without uncertainty or disturbance so it can be used as reference model in the control loop [79] [38].

The system is transformed into Byrnes-Isidori form as in equation 3.1; however, according to the relative degree obtained which is the same number of states ($r = n$) the internal dynamics $\dot{\eta}$ is not considered in the structure. This is an assumption that is a requirement in order to facilitate feedback linearization of multi-input multi-output (MIMO) nonlinear systems [42].

The aim is to track a reference signal asymptotically; therefore, the error states are considered for the formulation:

$$\xi_e^* = \xi^* - \xi_d \tag{3.15}$$

where:

ξ^* is the model state variable
ξ_d is desired state variable

It should be considered that for this stage of the design the linear change of coordinates in equation 3.11 are adapted to the variables of the Byrnes-Isidori form in equation 3.1. In consequence, the new state variable is ξ (external states Byrnes-Isidori form) which is considered different as the state ξ of the dynamic extension. Then the error dynamics in open loop is expressed as

$$\dot{\xi}_e^* = A\xi_e^* + B(a(\xi_d + \xi_e^*) + b(\xi_d + \xi_e^*)u^*) \tag{3.16}$$

Where the matrices:

$$a(\xi_d + \xi_e^*) = \begin{bmatrix} L_f^{r_1} h_1(\xi_d + \xi_e^*) \\ L_f^{r_2} h_2(\xi_d + \xi_e^*) \\ L_f^{r_3} h_3(\xi_d + \xi_e^*) \\ L_f^{r_4} h_4(\xi_d + \xi_e^*) \end{bmatrix} \tag{3.17}$$

$$b(\xi_d+\xi_e^*) = \begin{bmatrix} L_{g1}L_f^{r_1-1}h_1(\xi_d+\xi_e^*) & L_{g2}L_f^{r_1-1}h_1(\xi_d+\xi_e^*) & L_{g3}L_f^{r_1-1}h_1(\xi_d+\xi_e^*) & L_{g4}L_f^{r_1-1}h_1(\xi_d+\xi_e^*) \\ L_{g1}L_f^{r_2-1}h_2(\xi_d+\xi_e^*) & L_{g2}L_f^{r_2-1}h_2(\xi_d+\xi_e^*) & L_{g3}L_f^{r_2-1}h_2(\xi_d+\xi_e^*) & L_{g4}L_f^{r_2-1}h_2(\xi_d+\xi_e^*) \\ L_{g1}L_f^{r_3-1}h_3(\xi_d+\xi_e^*) & L_{g2}L_f^{r_3-1}h_3(\xi_d+\xi_e^*) & L_{g3}L_f^{r_3-1}h_3(\xi_d+\xi_e^*) & L_{g4}L_f^{r_3-1}h_3(\xi_d+\xi_e^*) \\ L_{g1}L_f^{r_4-1}h_4(\xi_d+\xi_e^*) & L_{g2}L_f^{r_4-1}h_4(\xi_d+\xi_e^*) & L_{g3}L_f^{r_4-1}h_4(\xi_d+\xi_e^*) & L_{g4}L_f^{r_4-1}h_4(\xi_d+\xi_e^*) \end{bmatrix} \tag{3.18}$$

The design for the control law:

$$u^* = b(\xi_d+\xi_e^*)^{-1}[-a(\xi_d+\xi_e^*)+v] \tag{3.19}$$

Then the nominal system input v can be designed as

$$v = K^*\xi_e^* \tag{3.20}$$

The selection of $K \in \mathbb{R}^{m\times n}$ is made to ensure the closed loop system $A+BK^*$ is Hurwitz:

$$\dot{\xi}_e^* = (A+BK^*)\xi_e^* \tag{3.21}$$

For the present work a it is enough to apply pole placement technique to ensure stability of the system.

In the next section the process controller is designed. The control input of the model will be implemented as feedforward control to the real system.

3.4. Process Control Loop

The process control loop (PCL) accounts for system disturbances and uncertainties. In this stage the design is developed by the error dynamics resulting from difference between the states of the process and the nominal model states. A controller based on feedback linearization with high-gain state feedback is employed to stabilize the system as commented in the objectives for the process control loop.

The error of states is defined for the process as in [76]:

$$\begin{aligned} \widetilde{\xi} &= \xi - \xi^* \\ &= \xi - \xi_d - \xi_e^* \end{aligned} \tag{3.22}$$

where:

ξ is the process state variable
ξ^* is the model state variable

Hence, the error dynamics in open loop for the process is expressed as

$$\dot{\widetilde{\xi}} = A\widetilde{\xi} + B\Big(\widetilde{a}(\xi_d + \xi_e^*, \widetilde{\xi}, u^*) + b(\xi_d + \xi_e^* + \widetilde{\xi})\widetilde{u} + \Psi(\xi_d + \xi_e^* + \widetilde{\xi})\Big) \tag{3.23}$$

where:

$$\Psi(\xi_d + \xi_e^* + \widetilde{\xi})$$

represents the uncertainty of the process.

Then the feedback linearization control law is designed as

$$\widetilde{u} = b(\xi_d + \xi_e^* + \widetilde{\xi})^{-1}[-\widetilde{a}(\xi_d + \xi_e^*, \widetilde{\xi}, u^*) + \tilde{v}] \tag{3.24}$$

and the linear input of the process $\tilde{v}$ is designed in the following manner:

$$\tilde{v} = \tilde{K}\widetilde{\xi}$$

Another state space feedback gain $\tilde{K} \in \mathbb{R}^{m \times n}$ is made to ensure the closed loop system $A + B\tilde{K}$ is Hurwitz where according to [45]

$$\tilde{K} = KD^{-1}\varepsilon^{-1}$$

D is a diagonal matrix:

$$D = diag(\varepsilon^{r-1}, \varepsilon^{r-2}, ..., 1)$$

and ε is positive constant between $0 < \varepsilon \leq 1$

The closed loop system for the process control is obtained as

$$\dot{\widetilde{\xi}} = (A + BK^*D^{-1}\varepsilon^{-1})\widetilde{\xi} + B\Psi(\xi_d + \xi_e^* + \widetilde{\xi}) \tag{3.25}$$

Then, using the transformation variable $\overline{\xi} = D^{-1}\widetilde{\xi}$ for time scaling in equation 3.25

$$\begin{aligned}
D^{-1}\dot{\widetilde{\xi}} &= D^{-1}(A + BK^*D^{-1}\varepsilon^{-1})\widetilde{\xi} + D^{-1}B\Psi(\xi_d + \xi_e^* + D\overline{\xi}) \\
\dot{\overline{\xi}} &= (D^{-1}A + D^{-1}BK^*D^{-1}\varepsilon^{-1})D\overline{\xi} + D^{-1}B\Psi(\xi_d + \xi_e^* + D\overline{\xi}) \\
\dot{\overline{\xi}} &= (D^{-1}AD + D^{-1}BK^*\varepsilon^{-1})\overline{\xi} + D^{-1}B\Psi(\xi_d + \xi_e^* + D\overline{\xi})
\end{aligned}$$

multiplying both sides of the equation by ε

$$\varepsilon\dot{\bar{\xi}} = \varepsilon(D^{-1}AD + D^{-1}BK^*\varepsilon^{-1})\bar{\xi} + \varepsilon D^{-1}B\Psi(\xi_d + \xi_e^* + D\bar{\xi})$$

with the simplification $D^{-1}B = B$ and $\varepsilon D^{-1}AD = A$ used in [76] then it is obtained:

$$\varepsilon\dot{\bar{\xi}} = (A + BK^*)\bar{\xi} + \varepsilon B\Psi(\xi_d + \xi_e^* + D\bar{\xi})$$

In this section the design of a model following control were developed using feedback linearization by implementing high-gain state feedback. The state space model was time scaled. In the next section the analysis of uncertainty will take place. A Lyapunov function is proposed for the analysis

3.5. Uncertainty Analysis

In this section it is considered the disturbances in the system. The gyroscopic effect τ_{gyro} mentioned in the modeling in equation 2.22 is incorporated to the attitude equations. Then, $f(x)$ of the nonlinear system is as follows:

$$f(x) = \begin{bmatrix} u_0 \\ v_0 \\ w_0 \\ qsin(\phi)sec(\theta) + rcos(\phi)sec(\theta) \\ qcos(\phi) - rsin(\phi) \\ p + qsin(\phi)tan(\theta) + rcos(\phi)tan(\theta) \\ 0 \\ 0 \\ g \\ \dfrac{I_y - I_z}{I_x}qr - \dfrac{I_r q\omega_r}{I_x} \\ \dfrac{I_z - I_x}{I_y}pr + \dfrac{I_r p\omega_r}{I_y} \\ \dfrac{I_x - I_y}{I_z}pq \end{bmatrix} \tag{3.26}$$

Consider the affine system with disturbance $\Psi_i(x)$

$$\dot{x} = f(x) + g(x)u + \Psi_(x)$$

and one output $y_1 = h_1(x)$. Consider the linear equation in 3.11 where the state variables are in z change of coordinates. Obtaining the first Lie derivative:

$$\begin{aligned}\frac{d}{dt}h_1(x) &= \frac{\partial h_1(x)}{\partial x}(f(x) + g(x)u + \Psi(x)) \\ &= L_f h_1(x) + L_g h_1(x)u + L_\Psi h_1(x) \\ &= z_2 + \Psi_{11}\end{aligned}$$

Then, the second Lie derivative is obtained:

$$\begin{aligned}\frac{d}{dt}L_f h_1(x) &= \frac{\partial L_f h_1(x)}{\partial x}(f(x) + g(x)u + \Psi_(x)) \\ &= L_f^2 h_1(x) + L_g L_f h_1(x)u + L_\Psi L_f h_1(x) \\ &= z_3 + \Psi_{12}\end{aligned}$$

Then the full system is:

$$\begin{aligned}\dot{z_1} &= z_2 + \Psi_{11} \\ \dot{z_2} &= z_3 + \Psi_{12} \\ \dot{z_3} &= z_4 + \Psi_{13} \\ \dot{z_4} &= v_5 + \Psi_{14} \\ \dot{z_5} &= z_6 + \Psi_{21} \\ \dot{z_6} &= z_7 + \Psi_{22} \\ \dot{z_7} &= z_8 + \Psi_{23} \\ \dot{z_8} &= v_2 + \Psi_{24} \\ \dot{z_9} &= z_{10} + \Psi_{31} \\ \dot{z_{10}} &= z_{11} + \Psi_{32} \\ \dot{z_{11}} &= z_{12} + \Psi_{33} \\ \dot{z_{12}} &= v_3 + \Psi_{34} \\ \dot{z_{13}} &= z_{14} + \Psi_{41} \\ \dot{z_{14}} &= v_4 + \Psi_{42}\end{aligned} \tag{3.27}$$

where $\Psi_{ij} = L_\Psi L_f^{j-1} h_i(x)$. Consider the system now in state space variables, the uncertainties

are solved:

$$\Psi_{14} = -\frac{I_r\omega_r x_{10}((1/I_y)x_{10}cos(x_4)cos(x_5) - (1/I_x)x_{11}cos(x_6)sin(x_4) + (1/I_y)x_{11}cos(x_4)sin(x_5)sin(x_6))}{m}$$

$$\Psi_{24} = -\frac{I_r\omega_r x_{10}((1/I_y)x_{10}cos(x_5)sin(x_4) + (1/I_x)x_{11}cos(x_4)cos(x_6) + (1/I_x)x_{11}sin(x_4)sin(x_5)sin(x_6))}{m}$$

$$\Psi_{34} = \frac{I_r\omega_r x_{10}((1/I_y)x_{10}sin(x_5) - (1/I_x)x_{11}cos(x_5)sin(x_6))}{m}$$

$$\Psi_{42} = \frac{I_r\omega_r(1/I_y)x_{10}sin(x_6)}{cos(x_5)} \tag{3.28}$$

These solutions were calculated via software using symbolic toolbox from Matlab. Then as expected the other terms a equal to zero. It should be marked that due to the feedback linearization, four linear subsystems were obtained. From the fourteen new coordinates, the first three groups of four equations belongs to the position x, y and z; and the last two equations correspond to the yaw attitude angle.

3.5.1. Analysis in the Model Control Loop

In the model control loop consider again the change of coordinates where z^* denotes errors in MCL

$$\dot{z}^* = (A + BK)z^* \tag{3.29}$$

then the Lyapunov function is proposed as

$$V^* = {z^*}_1^T P {z^*}_1 + {z^*}_2^T P {z^*}_2 + {z^*}_3^T P {z^*}_3 + {z^*}_4^T P_4 {z^*}_4 \tag{3.30}$$

There are four Lyapunov equations summed due to the four subsystems explained before. P is the solution of the Lyapunov equation (theory found in [36]) for the three axis positions (the matrices A and B are equal). P_4 is the solution of the Lyapunov equation for the yaw rotation.

From [36] the next relationships are obtained:

$$\dot{V^*} \leq -\frac{1}{\lambda_{max}(P)}V^*$$

where $\lambda_{max}(P)$ indicates the maximum eigenvalue of P. Then, the inequality:

$$\dot{V^*} \leq e^{-\frac{1}{\lambda_{max}(P)}(t-t_0)} V^*(t_0)$$

$$\lambda_{min}(P)\|z^*\|_2^2 \leq e^{-\frac{1}{\lambda_{max}(P)}(t-t_0)} \lambda_{max}(P)\|z^*(t_0)\|_2^2$$

$$\|z^*\|_2 \leq \sqrt{\frac{\lambda_{max}(P)}{\lambda_{min}(P)}} e^{-\frac{1}{\lambda_{max}(P)}(t-t_0)} \|z^*(t_0)\|_2^2$$

Then $\|z^*\|$ has its maximum at t_0 with:

$$\|z^*\|_2 \leq \sqrt{\frac{\lambda_{max}(P)}{\lambda_{min}(P)}} \|z^*(t_0)\|_2 \tag{3.31}$$

Therefore, $\|z^*\|$ is bounded and hence all model error states z_i^* are bounded.

3.5.2. Analysis in the Process Control loop

A lyapunov function in the process control loop (PCL) is proposed:

$$\overline{V} = \overline{z}_1^T P \overline{z}_1 + \overline{z}_2^T P \overline{z}_2 + \overline{z}_3^T P \overline{z}_3 + \overline{z}_4^T P_4 \overline{z}_4 \tag{3.32}$$

where $\overline{z}_i = D^{-1}\tilde{z}$ is time scaled concerning the errors of the PCL $\tilde{z}$. Then, from [76] the inequality of the derivative of the Lyapunov function:

$$\dot{\overline{V}} \leq -\epsilon^{-1}(\overline{z}_1^T \overline{z}_1 + \overline{z}_2^T \overline{z}_2 + \overline{z}_3^T \overline{z}_3 + \overline{z}_4^T \overline{z}_4) + 2(\|B^T P\|_2(\Psi_1 + \Psi_2 + \Psi_3) + \|B_4^T P_4\|_2 \Psi_4)\|\overline{z}\|_2 \tag{3.33}$$

Then, it can be simplified by the expression:

$$\dot{\overline{V}} \leq -\epsilon^{-1}(\|\overline{z}\|_2^2 + 2max\{\|B^T P\|_2, \|B_4^T P_4\|_2\}\|\Psi_0\|_2\|\overline{z}\|_2$$

where $\|\Psi_0\|_2 = \|\Psi_1\|_2 + \|\Psi_2\|_2 + \|\Psi_3\|_2 + \|\Psi_4\|_2$

The bound for the uncertainty:

$$\|\Psi\|_2 \leq \gamma(\|\overline{z}\|_2 + \|z^*\|_2)$$

$$\|\Psi\|_2 \leq \gamma(\|\overline{z}\|_2) + \gamma(\|z^*\|_2)$$

Using 3.31, then:

$$\|\Psi\|_2 \leq \|\overline{z}\|_2 + \sqrt{\frac{\lambda_{max}(P)}{\lambda_{min}(P)}}\|z^*(t_0)\|_2$$

This last expression can be replaced with $\delta > 0$

$$\|\Psi\|_2 \leq \gamma\|\overline{z}\|_2 + \delta \tag{3.34}$$

Multiplying by $2max\{\|B^TP\|_2, \|B_4^TP_4\|_2\}$ to the left and by $\|\overline{z}\|_2$ to the right the equation 3.34, it is obtained:

$$\begin{aligned} 2max\{\|B^TP\|_2, \|B_4^TP_4\|_2\}\|\Psi\|_2\|\overline{z}\|_2 \leq 2max\{\|B^TP\|_2, \|B_4^TP_4\|_2\}\gamma\|\overline{z}\|^{\ 2} \\ +2max\{\|B^TP\|_2, \|B_4^TP_4\|_2\}\delta\|\overline{z}\|_2 \end{aligned}$$

Adding the term $-\epsilon^{-1}\|\overline{z}\|_2^2$ in both sides of the inequality, it is obtained the following expression:

$$\begin{aligned} \dot{\overline{V}} \leq -\epsilon^{-1}\|\overline{z}\|_2^2 + 2max\{\|B^TP\|_2, \|B_4^TP_4\|_2\}\|\Psi_0\|_2\|\overline{z}\| \ \leq -\epsilon^{-1}\|\overline{z}\|_2^2 + 2max\{\|B^TP\|_2, \|B_4^TP_4\|_2\}\gamma\|\overline{z}\|_2^2 \\ +2max\{\|B^TP\|_2, \|B_4^TP_4\|_2\}\delta\|\overline{z}\|_2 \end{aligned}$$

Therefore, the inequality associated with the Lyapunov function derivative:

$$\dot{\overline{V}} \leq -(\epsilon^{-1} - 2max\{\|B^TP\|\_2, \|B_4^TP_4\|_2\}\gamma)\|\overline{z}\|_2^2 + 2max\{\|B^TP\|_2, \|B_4^TP_4\|_2\}\delta\|\overline{z}\|_2^2 \tag{3.35}$$

Then, for the stability it is required that

$$\epsilon^{-1} - 2max\{\|B^TP\|\_2, \|B_4^TP_4\|_2\}\gamma > 0$$

The bound for the uncertainty:

$$\gamma < \frac{1}{2\epsilon(max\{\|B^TP\|_2, \|B_4^TP_4\|_2\})}$$

To carry the analysis in the expression in 3.34 it should be noted that $\|\Psi\|_2$ is in x coordinates while the inequality should be taken in same coordinates as $\|\overline{z}\|_2$. In order to achieve that procedure, the inverse of the coordinates transformation $x = \Phi^{-1}(z)$ must be done. The expression was tried to do analytically and with computational tools; nevertheless the computation was to large and the simulation could not run due to the solutions of sixteen equations. Therefore, for the present work in a simulation and graphic sense were chosen to fulfill the inequality. Taking $\delta^* > 0$ enough large and then changing its values. This will be done in the simulation chapter.

Chapter 4

Simulations and results

In this section the tests for the proposed model following control system technique are performed through computer simulations using MATLAB® and Simulink software. Then, the results are analyzed. First of all, the model control loop is evaluated. The ideal system equations are implemented in function block. Then, the controller block is divided in static controller which the state feedback gain can be found and its outputs are connected to the feedback linearization dynamic controller with the dynamic extension which is represented by the double integrator. Second of all, the process control loop is added to the full system. The nonlinear dynamics with uncertainty model is considered as real process. This is developed in a function block, then the design of the process controller is implemented taking the structure of the model controller: the feedback linearization technique with dynamic extension, but with the high gain state feedback for the error dynamics.

4.1. Model Control Loop Simulation

The simulation is made in Simulink. The model control loop consists in three blocks: First, the "Nonlinear Quadrotor Model" where the dynamics of the quadrotor without disturbances is modeled by differential equations. Second, the "Static Control MCL" which is a state feedback gain that multiplies the nominal system error between the reference input and the states of the model previously coordinates transformed. Finally, the "Dynamic Control MCL" where the feedback linearization with dynamic extension is applied. The double integrators are part of the system corresponding to the augmented states. The description can be seen in Figure 4.1

According to transformed linear system obtained in equation 3.11 where the system matrix A in 3.12 and the input matrix B in 3.13 are constructed, the feedback gain matrix K^* in equation 3.20 can be solved. Pole placement design method was chosen because of its simplicity of the poles location in the Laplace plane.

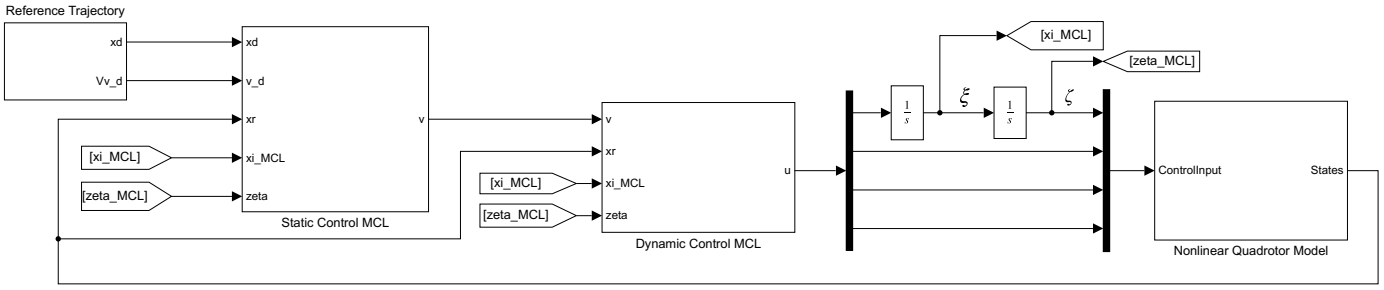

Figure 4.1: Model Control Loop structure in simulation environment.

The parameters involved in the present work are described in tables 4.1 , 4.2 and 4.3.

Due to A is a full linear system it can be decoupled in four independent subsystem as commented in the chapter before: three subsystems regarding the position coordinates x, y and z; and one more for the yaw rotation angle ψ. 14x14 matrix:

$$A_x = \begin{bmatrix} A_x & 0 & 0 & 0 \\ 0 & A_y & 0 & 0 \\ 0 & 0 & A_z & 0 \\ 0 & 0 & 0 & A_\psi \end{bmatrix} \tag{4.1}$$

Then, for x position movement:

$$A_x = \begin{bmatrix} 0 & 1 & 0 & 0 \\ 0 & 0 & 1 & 0 \\ 0 & 0 & 0 & 1 \\ 0 & 0 & 0 & 0 \end{bmatrix} \quad B_x = \begin{bmatrix} 0 \\ 0 \\ 0 \\ 1 \end{bmatrix} \tag{4.2}$$

The eigenvalues of A_x are located in 0 in Laplace plane. A state feedback gain makes the closed loop system stable. Then, placing the poles in -3, the feedback gain :

$$K_x^* = \begin{bmatrix} -81 & -108 & -54 & -12 \end{bmatrix} \tag{4.3}$$

The feedback gain K_x^* is used also for the position y and z due to the same dynamics. For the dynamics of the yaw rotation A_ψ is a 2x2 matrix and the poles were also located in -6. Then the feedback gain:

$$K_\psi^* = \begin{bmatrix} -9 & -6 \end{bmatrix} \tag{4.4}$$

Parameter	Comment	Unit
x_0	translational position about x axis	m
y_0	translational position about y axis	m
z_0	translational position about z axis	m
u	translational velocity in x axis	m/s
v	translational velocity in y axis	m/s
w	translational velocity in z axis	m/s
ϕ	roll angle	rad
θ	pitch angle	rad
ψ	yaw angle	rad
p	angular rate around x axis	rad/s
q	angular rate around y axis	rad/s
r	angular rate around z axis	rad/s
I_x	Moment of inertia about x axis	Kgm^2
I_y	Moment of inertia about y axis	Kgm^2
I_z	Moment of inertia about z axis	Kgm^2

Table 4.1: Parameters for the quadrotor.

Parameter	Comment	Unit
T	Thrust force	N
τ_ϕ	Roll torque	Nm
τ_θ	Pitch torque	Nm
τ_ψ	Yaw torque	Nm

Table 4.2: Control inputs of the quadrotor.

Parameter	Comment	Value	Unit
m	Mass	0.4794	Kg
g	Gravity	9.81	m/s^2
l	Frame length	0.225	m
I_x	Moment of inertia about x axis	0.0086	Kgm^2
I_y	Moment of inertia about y axis	0.0086	Kgm^2
I_z	Moment of inertia about z axis	0.0172	Kgm^2
I_r	Total moment of inertia of the propellers	3.7404×10^{-5}	Kgm^2
k	Thrust coefficient	3.13×10^{-5}	–
d	Drag coefficient	9×10^{-7}	–

Table 4.3: Parameters of quadrotor for simulations. The parameters used in this work are based on [28] .

For the simulation a trajectory is chosen to be follow which are the desired states vectors:

$$
\begin{aligned}
x_{0d} &= 1.5\ sin(t) \\
y_{0d} &= 1.5\ cos(t) \\
z_{0d} &= 1.4\ t \\
\psi_d &= \pi/6
\end{aligned}
$$

The position output response is indicated by blue color and the red trajectory is the reference input to be followed. In the Figure 4.2 it can be seen that the parth is followed by the output response in all axis. Due to the trajectory is a spiral the results in each axis can be shown as sine and cosine signals in coordinates x and y respectively and a ramp signal for the z coordinate as the quadrotor is elevating.

The simulation also shows the three Euler angles. ψ is the only angle to be controlled and it follows the step reference input as shown in Figure 4.3. The values of the angles θ and ϕ are between -0.2 and 0.2 radians which are between the range indicated in the modeling. Then, the four outputs were controlled and could follow the desired trajectories.

The control effort u_1 Thrust force and the roll, pitch and yaw torques are shown in Figure 4.4 for the model control loop. One can observe that the torques converge to zero due to the equilibrium Torque during the flight.

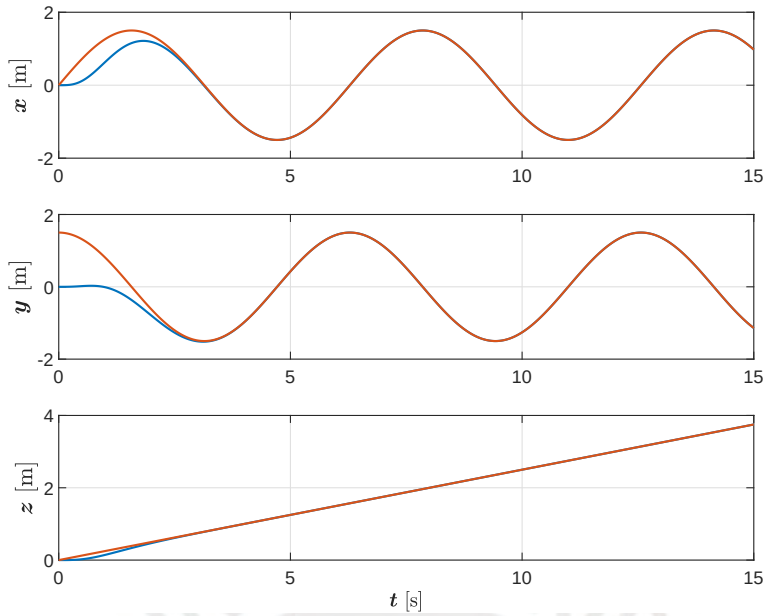

Figure 4.2: Position response in Model Control Loop

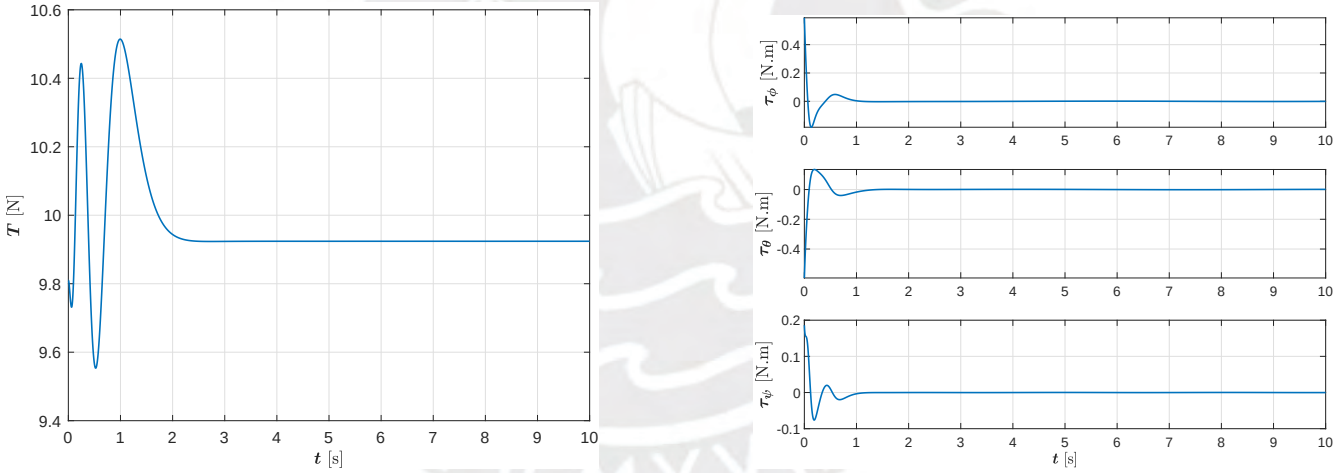

(a) Thrust control input

(b) Attitude torques

Figure 4.4: Quadrotor control signals

In Figure 4.5 it can be visualized the desired trajectory and the trajectory generated by the MCL block.

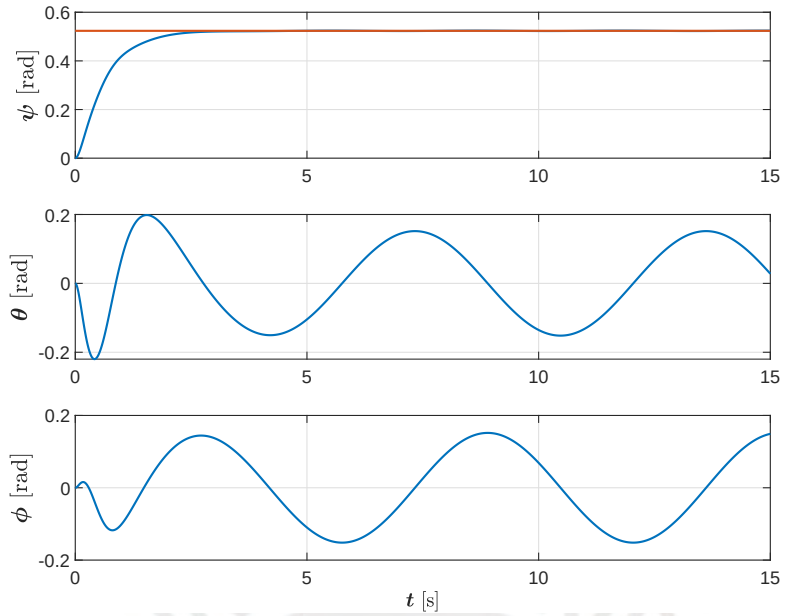

Figure 4.3: Euler angles response in Model Control Loop

4.2. Process Control Loop Simulation

In order to design the Process Control Loop, The nonlinear system with disturbances is considered. For this work the gyroscopic effect was added. The implementation of the system can be seen in Figure 4.6. It can be shown the MCL and the PCL working in whole system where the dynamic extension by two integrators were applied for both blocks due to the feedback linearization. As in equation 3.26 the term $\omega_r = \omega_1 + \omega_2 + \omega_3 + \omega_4$ is in the gyroscopic effect. This was also implemented for the PCL by the following formulation taken from equation 2.21 and the Thrust:

The four equations can be written in matrix form as:

$$\begin{bmatrix} \tau_\phi \\ \tau_\theta \\ \tau_\psi \\ T \end{bmatrix} = \begin{bmatrix} 0 & -lk & 0 & lk \\ -lk & 0 & lk & 0 \\ b & -b & b & -b \\ k & k & k & \end{bmatrix} \begin{bmatrix} \omega_1^2 \\ \omega_2^2 \\ \omega_3^2 \\ \omega_4^2 \end{bmatrix} \tag{4.5}$$

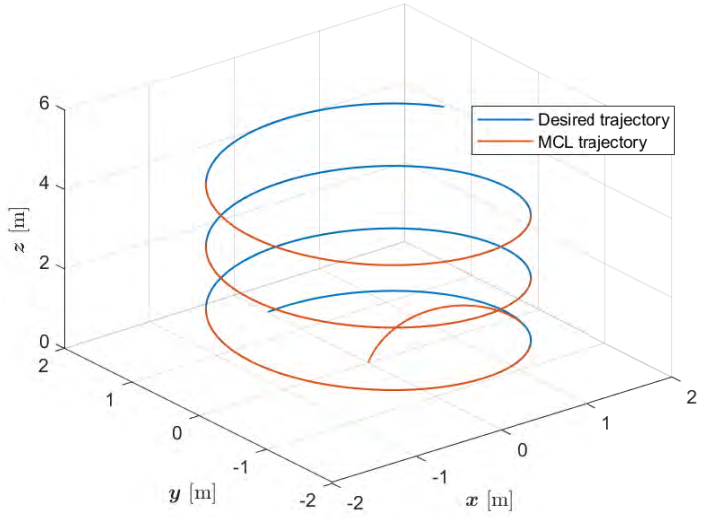

Figure 4.5: Trajectory followed using feedback linearization in the MCL. This indicates that the quadrotor model follows the desired trajectory.

Taking the inverse of the matrix, the vector for the velocities can be obtained:

$$\begin{bmatrix} \omega_1^2 \\ \omega_2^2 \\ \omega_3^2 \\ \omega_4^2 \end{bmatrix} = \begin{bmatrix} 0 & -\frac{1}{2lk} & \frac{1}{4b} & \frac{1}{4k} \\ -\frac{1}{2lk} & 0 & -\frac{1}{4b} & \frac{1}{4k} \\ 0 & \frac{1}{2lk} & \frac{1}{4b} & \frac{1}{4k} \\ \frac{1}{2lk} & 0 & -\frac{1}{4b} & \frac{1}{4k} \end{bmatrix} \begin{bmatrix} \tau_\phi \\ \tau_\theta \\ \tau_\psi \\ T \end{bmatrix} \tag{4.6}$$

Then, the angular velocities for each motor so that the resultant ω_r can be obtained:

$$\omega_1 = \sqrt{-\frac{\tau_\theta}{2lk} + \frac{\tau_\psi}{4b} + \frac{T}{4k}}$$
$$\omega_2 = \sqrt{-\frac{\tau_\phi}{2lk} - \frac{\tau_\psi}{4b} + \frac{T}{4k}}$$
$$\omega_3 = \sqrt{-\frac{\tau_\theta}{2lk} + \frac{\tau_\psi}{4b} + \frac{T}{4k}}$$
$$\omega_4 = \sqrt{\frac{\tau_\phi}{2lk} - \frac{\tau_\psi}{4b} + \frac{T}{4k}}$$

The first simulation was made so that the poles of the PCL are 5 times faster than the poles

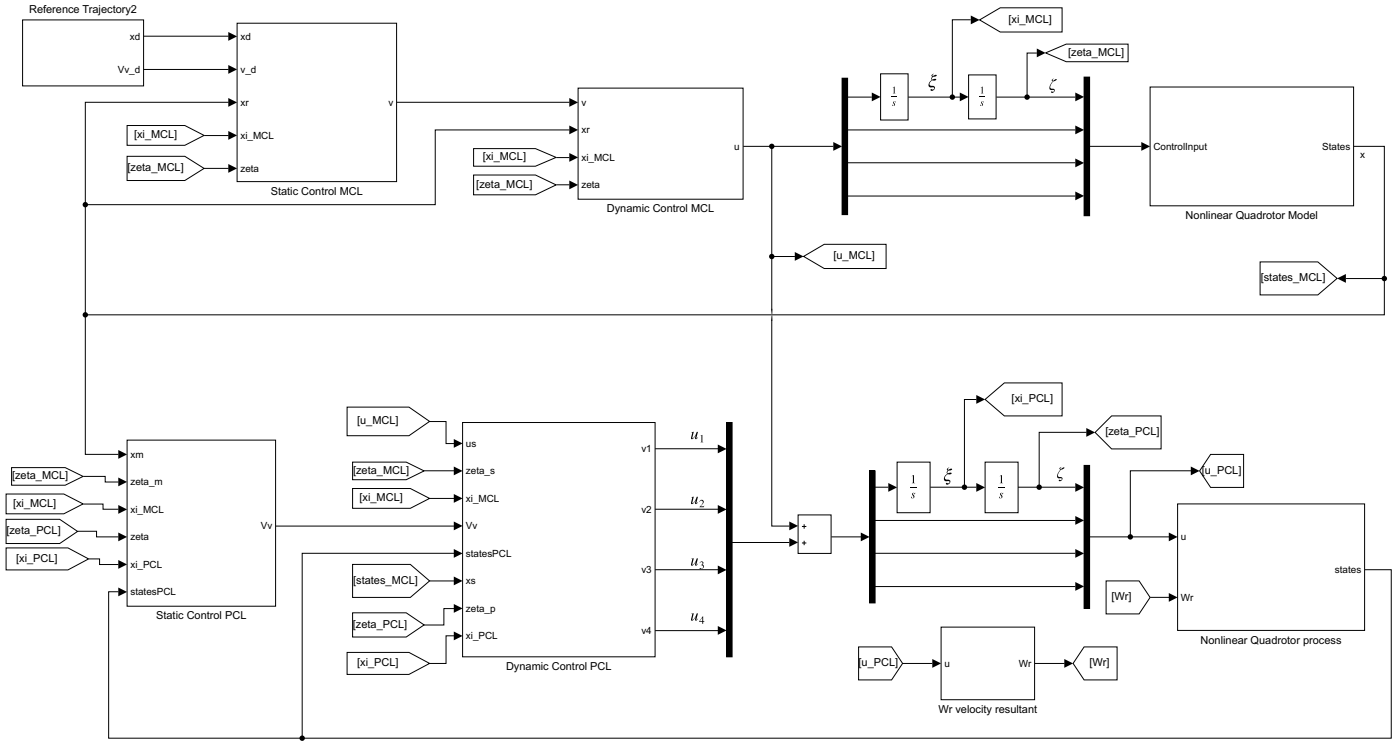

Figure 4.6: Model Following Control Simulation Diagram.

of the MCL. The theorem applied in [76] is used for the location of the poles:

$$\lambda_{PCL} = \frac{\lambda_{MCL}}{\epsilon}$$

$0 < \epsilon < 1$. So $\epsilon = 0.2$ in order to obtain the feedback gain of the PCL the eigenvalues have to be faster than the poles in MCL. Then, in Figure 4.7 it can be seen that the PCL controller made the system with disturbances follow the reference which were the outputs of the MCL.

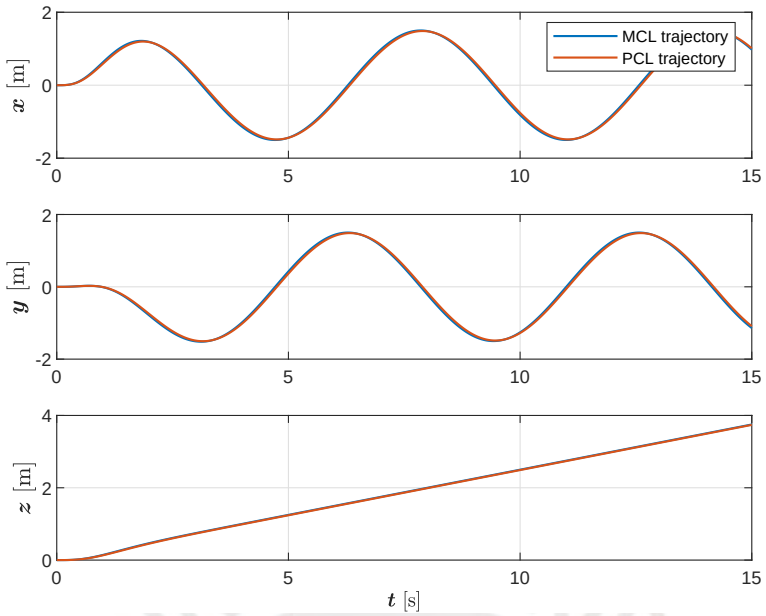

Figure 4.7: Position response in Process Control Loop. It can be noticed good tracking with all PCL poles located in $\lambda_{PCL} = -15$

The Euler angles were simulated as well. It is evident that the desired yaw angle is followed in Figure 4.8. For the angles pitch and roll there were no controlled, but as shown they have similar dynamic of the MCL and they are inside the range to avoid singularities.

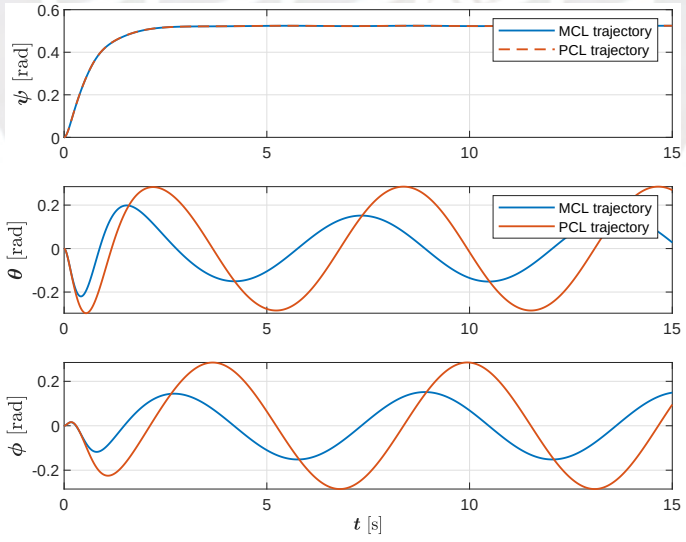

Figure 4.8: Euler angles in MCL and PCL of the quadrotor. With this information the attitude information of the aircraft can be obtained.

The simulation of the control inputs of PCL against MCL is shown in Figure 4.9. For the

Thrust force u_1 in PCL it can be seen that it requires less effort than the control in MCL. In the Torques graphics the signals behave similar.

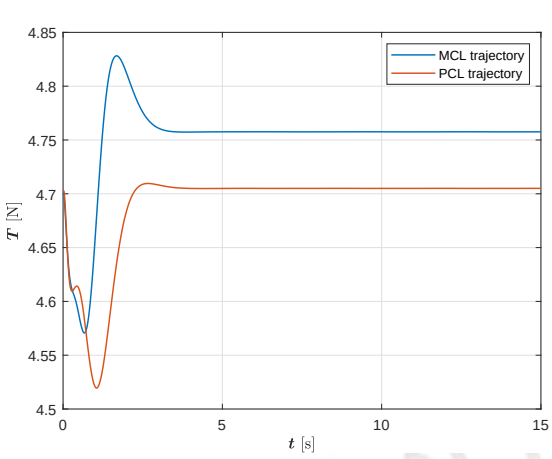

(a) Comparison of control effort in MCL y PCL.

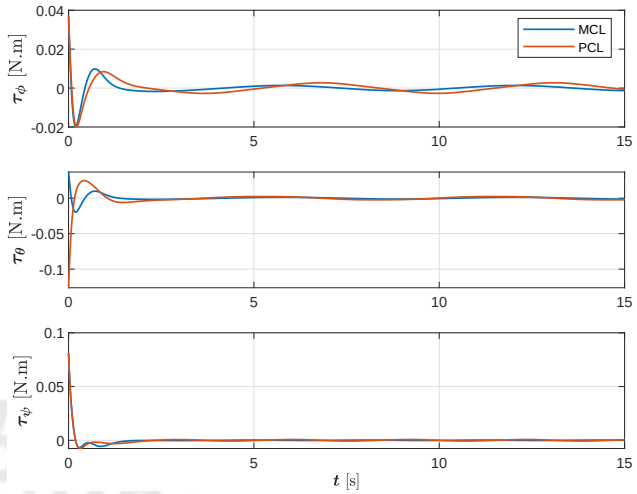

(b) Attitude torques in MCL and PCL

Figure 4.9: Quadrotor control inputs comparison in MCL and PCL

The next simulation the poles of the PCL were chosen faster and also changing the parameter ϵ. These simulations were contrasted with a single loop feedback linearization controller applied to the same nonlinear system.

In Figure 4.10 the poles for the MFC are seven times faster $\lambda_{PCL} = 7\lambda_{MCL}$. That means $\epsilon = 0.1429$ and in Figure 4.11 the Euler angles can be seen that the rotation movements are quite similar.

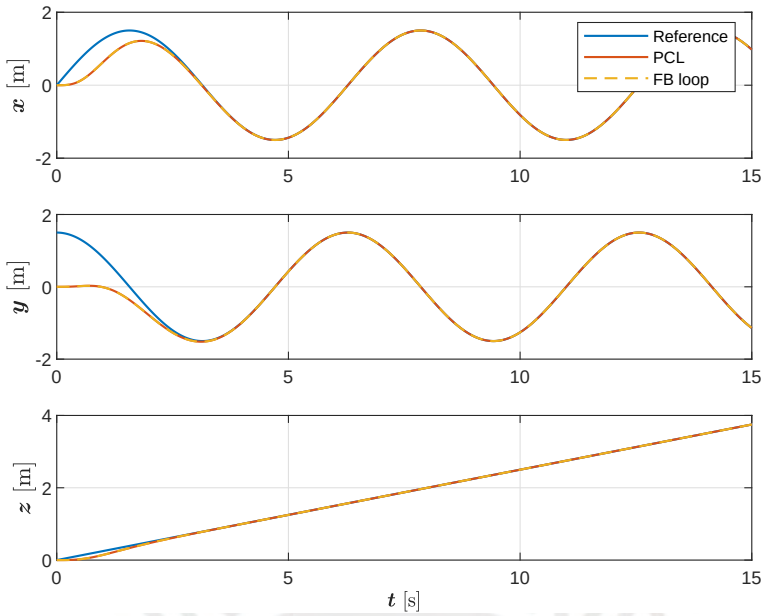

Figure 4.10: The PCL makes a better tracking as well the Feedback linearization one loop

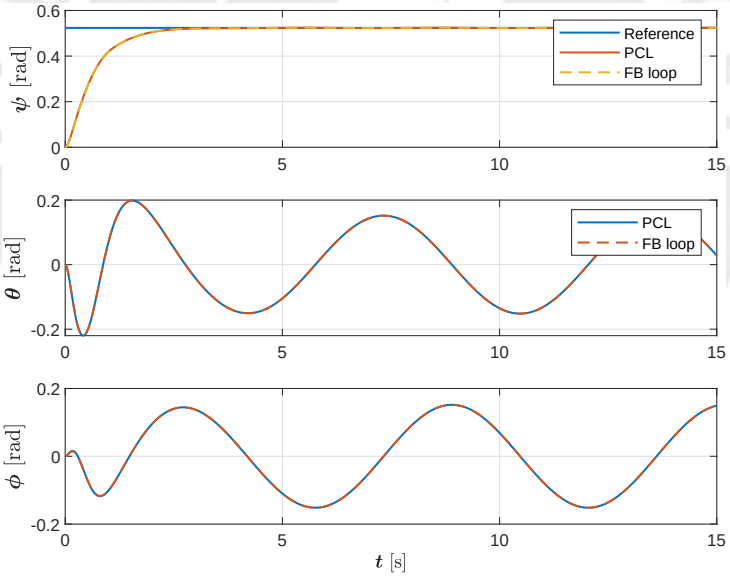

Figure 4.11: Euler angles in PCL and in feedback linearization loop has the same behavior in the quadrotor.

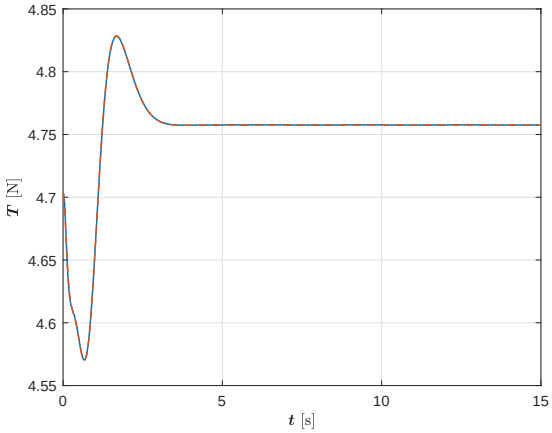

(a) Comparison of control effort in MCL y PCL.

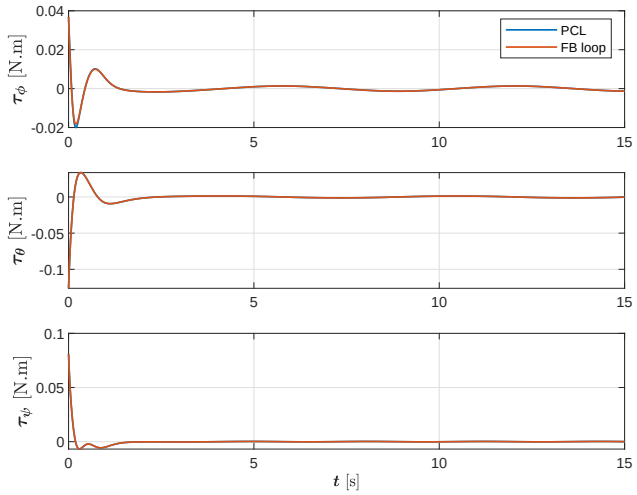

(b) Attitude torques in MCL and PCL

Figure 4.12: Quadrotor control inputs comparison PCL and one FB loop

Even the control law are very similar for the test. More simulations were made and the tracking for the MFC and the one loop feedback linearization work the same behavior. Then, it is proposed to add disturbance in other states such as wind behavior in each axis position and make tests.

In Figure 4.13 the poles were taken as same condition for the MFC seven times faster $\lambda_{PCL} = 7\lambda_{MCL}$ with $\epsilon = 0.1429$. The tracking is much better for the PCL than the FB lopp; nevertheless in Figure 4.14 it is clear that the control signal for the PCL is greater than FB loop

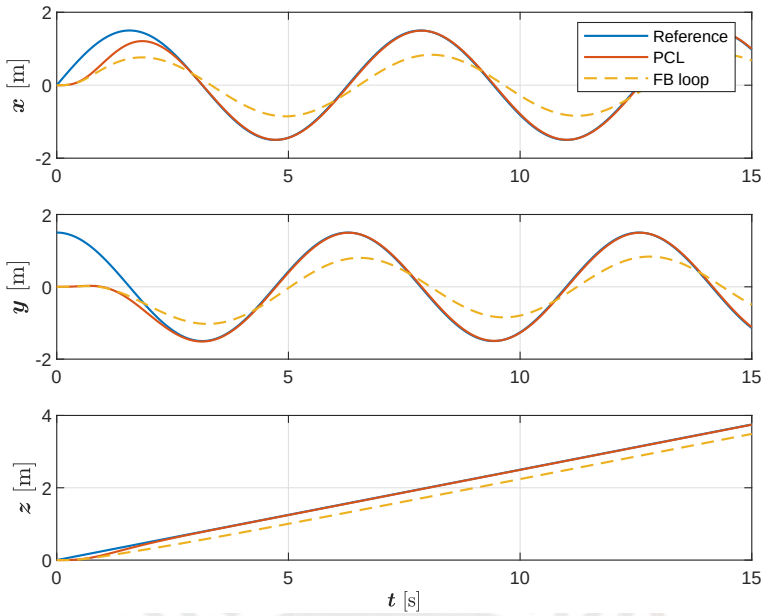

Figure 4.13: Position response in Process Control Loop. It can be noticed good tracking with all PCL poles located in $\lambda_{PCL} = -15$

The control input

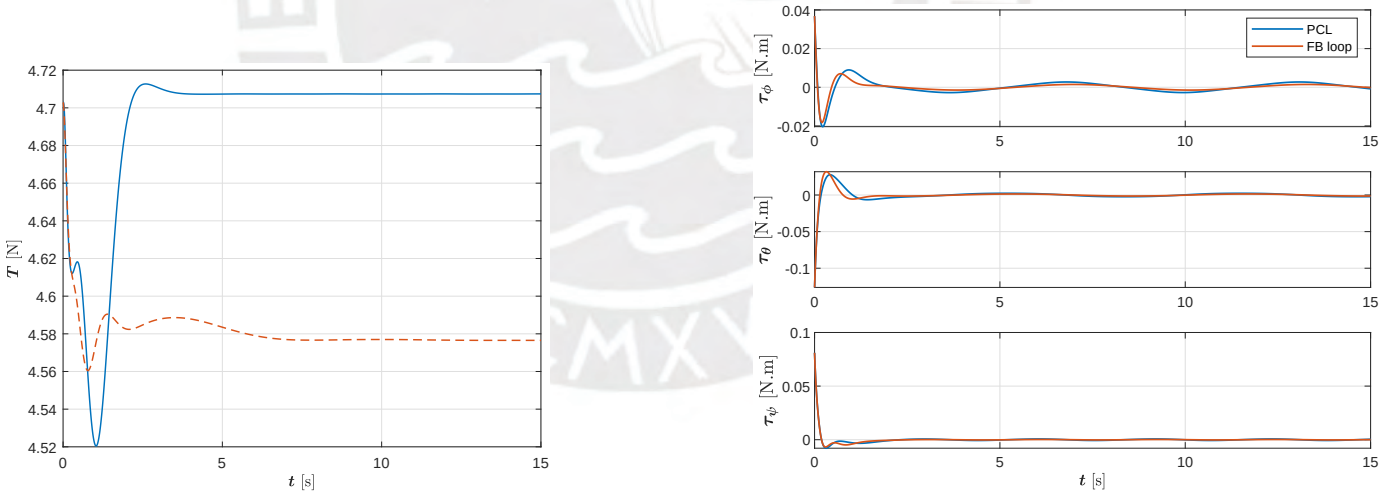

(a) Comparison of control effort PCL and FB loop.

(b) Attitude torques in PCL and FB Loop

Figure 4.14: Quadrotor control inputs comparison PCL and FB Loop

The verification of the inequality in 3.34 is made via simulation and it is shown in Figure

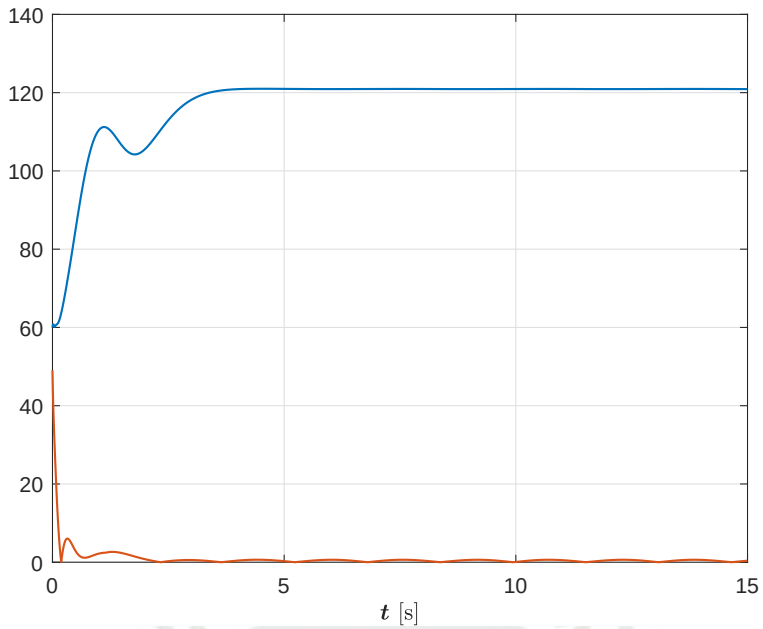

Figure 4.15: Comparison the uncertainty and states in z coordinates graphically where $\gamma = 3$ and $\delta = 60$

It can be seen that the initial value of $\gamma\|\overline{z}\|_2 + \delta$ is 60 then it can cover of the function $\|\Psi\|_2$ through time. The value of δ can be changed to have a better relationship but always greater than the initial value of the norm of the states in z coordinates.

4.2.1. Lyapunov Function Implementation

The proposed Lyapunov Function like in [76] is :

$$V = k{z_e^*}^T P z_e^* + {\overline{z}_e}^T P \overline{z}_e \tag{4.7}$$

where z_e^* and $\overline{z}_e$ represent the errors of change of coordinates in the MCL and PCL time scaled, respectively. The time scaled vector is equivalent to $\overline{z}_e = D^{-1}\overline{z}_e$, then:

$$V = k{z_e^*}^T P z_e^* + \tilde{z}_e^T D^{-1} P D^{-1} \tilde{z}_e \tag{4.8}$$

In this work there are four subsystems: three of them related to the positions x, y and z; and one for the angle ψ as indicated before, then four Lyapunov functions are proposed for each subsystem which are summed:

$$V = V_1 + V_2 + V_3 + V_4$$

where:

$$V_1 = k{z_{11}^*}^T P z_{11}^* + \tilde{z}_{11}^T D^{-1} P D^{-1} \tilde{z}_{11}$$
$$V_2 = k{z_{22}^*}^T P z_{22}^* + \tilde{z}_{22}^T D^{-1} P D^{-1} \tilde{z}_{22}$$
$$V_3 = k{z_{33}^*}^T P z_{33}^* + \tilde{z}_{33}^T D^{-1} P D^{-1} \tilde{z}_{33}$$
$$V_4 = k{z_{44}^*}^T P_4 z_{44}^* + \tilde{z}_{44}^T D_2^{-1} P_4 D_2^{-1} \tilde{z}_{44}$$

Where $P \in \mathbb{R}^4$ and $P_4 \in \mathbb{R}^2$ are the solutions of Lyapunov equation. Then, the matrices D and D_2 are such as:

$$D = diag(\varepsilon^{r_1-1}, \varepsilon^{r_1-2}, ..., 1)$$

r_1 relative degree four and

$$D_2 = diag(\varepsilon^{r_2-1}, \varepsilon^{r_2-2})$$

r_2 relative degree two

These four Lyapunov functions are simulated via software. In Figure 4.16 it is shown the four functions summed and it can be seen that is a positive definite function that was decreasing and stays in positive value that prove stability of the system.

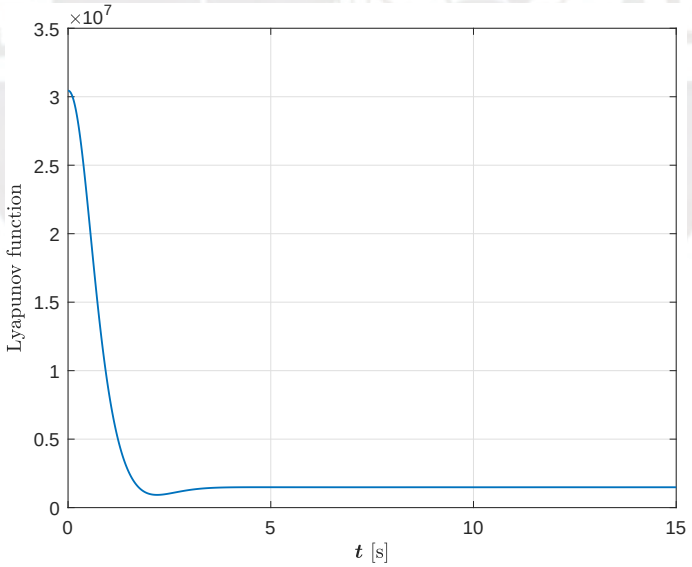

Figure 4.16: Simulated Lyapunov function for $\epsilon = 0.2$ which means the PCL five times faster than the MCL.

Chapter 5

Conclusions and Future Work

This master thesis was focused on the design and simulation of a model following controller for a quadrotor underactuated system as main object. A nonlinear model without simplifications was consider in affine form using kinematics and Newton-Euler rigid body formulation. The input signals were the attitude torques and the thrust, the output states to control were the three axis position and yaw angle. To carry out the design in the model control loop the model was considered nominal and a feedback linearization based on the error dynamics was designed. Dynamic extension case was applied to obtain the decoupling matrix nonsingular and achieve the relative degree. The simulations showed that the model control loop system could follow the reference trajectory. This was shown also in the trajectories of each axis dimension and the yaw angle individually. Then, a second controller, where the system was considered with external disturbances, was designed for the process control loop: feedback linearization with high-gain based on error dynamics. Due to this technique, uncertainty analysis was made for robustness performance. The proposed model following control approach with high-gain controller in the process control loop is capable to compensate model uncertainties with the feedback linearization technique when the uncertainty model is changed. It had better performance than the normal single-loop feedback linearization, but as shown in the simulations the control effort is required more. for the analysis of the inequality uncertainty the states were in z coordinates required; nevertheless, the analytical part was hard and large due to extensive calculations. This process was taken to the symbolical calculation and the simulation could not run since the equation solutions were too long. Then, the inequality was made graphically in the simulation and it is fulfilled.

As future work it is considered other nonlinear control algorithms like sliding mode control or backstepping and analyze the stability in the model following control structure. Make an strong mathematical analysis for the uncertainty is also considered. Then simulations with Gaussian noise is pretended to see how the system responds. After simulations and to prove this work it is thought of make the implementation of the algorithm in a microcontroller to make experimental flight tests on board.

Bibliography

[1] S. Abdelhay and A. Zakriti, "Modeling of a quadcopter trajectory tracking system using PID controller," *Procedia Manufacturing*, vol. 32, pp. 564–571, 2019.

[2] H. Agrawal, P. M. Tiwari, and N. Verma, "A chattering mitigating sliding mode control for rigid spacecraft attitude control maneuver," in *2020 International Conference on Advances in Computing, Communication & Materials (ICACCM)*. IEEE, aug 2020.

[3] F. Ahmad, P. Kumar, R. Dobriyal, and P. P. Patil, "Estimation of the thrust coefficient of a quadcopter propeller using computational fluid dynamics," *IOP Conference Series: Materials Science and Engineering*, vol. 1116, no. 1, p. 012095, apr 2021.

[4] A. Alaimo, V. Artale, C. Milazzo, A. Ricciardello, and L. Trefiletti, "Mathematical modeling and control of a hexacopter," in *2013 International Conference on Unmanned Aircraft Systems (ICUAS)*. IEEE, may 2013.

[5] M. Asnafi and S. Dastgheibifard, "A review on potential applications of unmanned aerial vehicle for construction industry," *Sustainable Structures and Materials, An International Journal*, vol. 1, pp. 44–53, 2018.

[6] P. Banerjee, *ISC Physics Book 1 XI*. S. Chand Publishing. [Online]. Available: https://books.google.de/books?id=KEZxEAAAQBAJ

[7] A. Benaddy, M. Labbadi, and M. Bouzi, "Robust super twisting terminal sliding mode tracking control for a quadrotor UAV with disturbances in discrete-time," in *2022 10th International Conference on Systems and Control (ICSC)*. IEEE, nov 2022.

[8] C. Berbra, S. Lesecq, S. Gentil, and J.-M. Thiriet, "CO-DESIGN OF a SAFE NETWORK CONTROL QUADROTOR," *IFAC Proceedings Volumes*, vol. 41, no. 2, pp. 5506–5511, 2008.

[9] V. Brito, A. Brito, L. B. Palma, and P. Gil, "Quadcopter control approaches and performance analysis," in *Proceedings of the 15th International Conference on Informatics in Control, Automation and Robotics*. SCITEPRESS - Science and Technology Publications, 2018.

[10] Z. Cai, S. Zhang, and X. Jing, "Model predictive controller for quadcopter trajectory tracking based on feedback linearization," *IEEE Access*, vol. 9, pp. 162 909–162 918, 2021.

[11] T. G. Carreira, "Quadcopter automatic landing on a docking station," 10 2013.

[12] E. Ciampa, L. D. Vito, and M. R. Pecce, "Practical issues on the use of drones for construction inspections," *Journal of Physics: Conference Series*, vol. 1249, no. 1, p. 012016, may 2019.

[13] D. Cobb and J. Eapen, "High-gain state feedback analysis based on singular system theory," in *Proceedings of the 45th IEEE Conference on Decision and Control*. IEEE, 2006.

[14] M. Collotta, G. Pau, and R. Caponetto, "A real-time system based on a neural network model to control hexacopter trajectories," in *2014 International Symposium on Power Electronics, Electrical Drives, Automation and Motion*. IEEE, 2014.

[15] J. J. Craig, *Robotica*. Pearson Educacion, 2008.

[16] A. Das, F. L., and K. Subbarao, "Sliding mode approach to control quadrotor using dynamic inversion," in *Challenges and Paradigms in Applied Robust Control*. InTech, nov 2011.

[17] M. Dhaybi and N. Daher, "Real-time estimation of the inertia tensor elements of a quadcopter hover platform," in *2019 IEEE/ASME International Conference on Advanced Intelligent Mechatronics (AIM)*. IEEE, jul 2019.

[18] G. Dutta and P. Goswami, "Application of drone in agriculture: A review," *International Journal of Chemical Studies*, vol. 8, no. 5, pp. 181–187, oct 2020.

[19] A. M. Elhennawy and M. K. Habib, "Trajectory tracking of a quadcopter flying vehicle using sliding mode control," in *IECON 2017 - 43rd Annual Conference of the IEEE Industrial Electronics Society*. IEEE, oct 2017.

[20] M. Esmail, M. Merzban, A. A. M. Khalaf, and H. Hamed, "Comparison of various control techniques applied to a quadcopter," *Journal of Advanced Engineering Trends*, vol. 42, no. 2, pp. 233–244, jul 2023.

[21] S. Feroz and S. A. Dabous, "UAV-based remote sensing applications for bridge condition assessment," *Remote Sensing*, vol. 13, no. 9, p. 1809, may 2021.

[22] Z. Gacovski, S. Deskovski, and V. Sazdovski, "Advanced guidance laws and navigation systems for uav: Theoretical and practical findings in a developing country," *Advances in Complex Systems*, 09 2011.

[23] O. Gehan, E. Pigeon, T. Menard, M. Pouliquen, H. Gualous, Y. Slamani, and B. Tala-Ighil, "A nonlinear state feedback for DC/DC boost converters," *Journal of Dynamic Systems, Measurement, and Control*, vol. 139, no. 1, oct 2016.

[24] M. K. Ghaffar, F. S. Fadhel, and N. E. Arif, "Application of the generalized backstepping control method for lotka-volterra prey-predator system with constant time delay," *Journal of Physics: Conference Series*, vol. 2322, no. 1, p. 012012, aug 2022.

[25] J. Ghandour, S. Aberkane, and J.-C. Ponsart, "Feedback linearization approach for standard and fault tolerant control: Application to a quadrotor UAV testbed," *Journal of Physics: Conference Series*, vol. 570, no. 8, p. 082003, dec 2014.

[26] W. Ghozlane and J. Knani, "Nonlinear control of mimo system using feedback linearization control method and pd controller for tracking purpose," 07 2018.

[27] A. Hafeez, M. A. Husain, S. Singh, A. Chauhan, M. T. Khan, N. Kumar, A. Chauhan, and S. Soni, "Implementation of drone technology for farm monitoring & pesticide spraying: A review," *Information Processing in Agriculture*, vol. 10, no. 2, pp. 192–203, jun 2023.

[28] Z. He and L. Zhao, "A simple attitude control of quadrotor helicopter based on ziegler-nichols rules for tuning PD parameters," *The Scientific World Journal*, vol. 2014, pp. 1–13, 2014.

[29] D. Hernandez, J.-C. Cano, F. Silla, C. T. Calafate, and J. M. Cecilia, "AI-enabled autonomous drones for fast climate change crisis assessment," *IEEE Internet of Things Journal*, vol. 9, no. 10, pp. 7286–7297, may 2022.

[30] D. Ho, *Some results on closed-loop identification of quadcopters*, ser. Linköping Studies in Science and Technology. Licentiate Thesis. Linköping University Electronic Press, 2018. [Online]. Available: https://books.google.de/books?id=kdV7DwAAQBAJ

[31] F. Hoffmann, N. Goddemeier, and T. Bertram, "Attitude estimation and control of a quadrocopter," in *2010 IEEE/RSJ International Conference on Intelligent Robots and Systems*. IEEE, oct 2010.

[32] M. Idrissi, F. Annaz, and M. Salami, "Mathematical & physical modelling of a quadrotor UAV," in *2021 7th International Conference on Control, Automation and Robotics (ICCAR)*. IEEE, apr 2021.

[33] A. Isidori, *Nonlinear Control Systems An Introduction*. Springer Berlin Heidelberg, 1989.

[34] M. Kedzierski, D. Wierzbicki, A. Sekrecka, A. Fryskowska, P. Walczykowski, and J. Siewert, "Influence of lower atmosphere on the radiometric quality of unmanned aerial vehicle imagery," *Remote Sensing*, vol. 11, no. 10, p. 1214, may 2019.

[35] P. Kemao, D. Miaobo, M. C. Ben, C. Guowei, L. K. Yew, and H. L. Tong, "Design and implementation of a fully autonomous flight control system for a UAV helicopter," in *2007 Chinese Control Conference*. IEEE, jul 2006.

[36] H. K. Khalil, *Nonlinear Control*. Pearson.

[37] K. Konstantoudakis, K. Christaki, D. Tsiakmakis, D. Sainidis, G. Albanis, A. Dimou, and P. Daras, "Drone control in ar: An intuitive system for single-handed gesture control, drone tracking, and contextualized camera feed visualization in augmented reality," *Drones*, vol. 6, no. 2, p. 43, feb 2022.

[38] J. kun LIU and F. chun SUN, "Nominal model-based sliding mode control with backstepping for 3-axis flight table," *Chinese Journal of Aeronautics*, vol. 19, no. 1, pp. 65–71, feb 2006.

[39] A. Lebedev, "Design and implementation of a 6dof control system for an autonomous quadrocopter," 09 2013.

[40] C. Lee, S. Kim, and B. Chu, "A survey: Flight mechanism and mechanical structure of the UAV," *International Journal of Precision Engineering and Manufacturing*, vol. 22, no. 4, pp. 719–743, 2021.

[41] H. Li, Z. Wang, Z. Xu, X. Wang, and Y. Hu, "Feedback linearization based direct torque control for IPMSMs," *IEEE Transactions on Power Electronics*, vol. 36, no. 3, pp. 3135–3148, mar 2021.

[42] Y. Li, M. Zeng, H. An, and C. Wang, "Disturbance observer-based control for nonlinear systems subject to mismatched disturbances with application to hypersonic flight vehicles," *International Journal of Advanced Robotic Systems*, vol. 14, no. 2, p. 172988141769914, mar 2017.

[43] A. Lushimba and J. Nackoney, "Using drone for surveillance and wildlife monitoring: Methodological approach in dja faunal reserve (cameroon)," 2019.

[44] S. Mansoor and M. Saedan, "Software-in-the-loop simulation of a quadcopter portion for hybrid aircraft control," *IOP Conference Series: Materials Science and Engineering*, vol. 297, p. 012044, jan 2018.

[45] R. Marino, "High-gain stabilization and partial feedback linearization," in *1986 25th IEEE Conference on Decision and Control*. IEEE, dec 1986.

[46] A. Misra, S. Jayachandran, S. Kenche, A. Katoch, A. Suresh, E. Gundabattini, S. K. Selvaraj, and A. A. Legesse, "A review on vertical take-off and landing (VTOL) tilt-rotor and tilt wing unmanned aerial vehicles (UAVs)," *Journal of Engineering*, vol. 2022, pp. 1–27, 2022.

[47] V. Mistler, A. Benallegue, and N. M'Sirdi, "Exact linearization and noninteracting control of a 4 rotors helicopter via dynamic feedback," in *Proceedings 10th IEEE International Workshop on Robot and Human Interactive Communication. ROMAN 2001 (Cat. No.01TH8591)*. IEEE.

[48] A. Nemati and M. Kumar, "Modeling and control of a single axis tilting quadcopter," in *2014 American Control Conference*. IEEE, jun 2014.

[49] D. D. Nguyen, J. Rohacs, and D. Rohacs, "Autonomous flight trajectory control system for drones in smart city traffic management," *ISPRS International Journal of Geo-Information*, vol. 10, no. 5, p. 338, may 2021.

[50] R. Niemiec and F. Gandhi, "A comparison between quadrotor flight configurations," 2016.

[51] L. Oliveira, A. Bento, V. J. Leite, and F. Gomide, "Comparisons of robust methods on feedback linearization through experimental tests," *IFAC-PapersOnLine*, vol. 53, no. 2, pp. 7983–7988, 2020.

[52] A. Oosedo, , H. Hattori, I. Yasui, and K. Harada, "Unmanned aircraft system traffic management (UTM) simulation of drone delivery models in 2030 japan," *Journal of Robotics and Mechatronics*, vol. 33, no. 2, pp. 348–362, apr 2021.

[53] T. Pajchrowski, "Robust control of PMSM system using the structure of MFC," *COMPEL - The international journal for computation and mathematics in electrical and electronic engineering*, vol. 30, no. 3, pp. 979–995, may 2011.

[54] T. Pengliang, "Feedback linearization of mimo nonlinear system with measurable disturbance," in *2020 12th International Conference on Measuring Technology and Mechatronics Automation (ICMTMA)*. IEEE, feb 2020.

[55] D. Rakesh, N. A. Kumar, M. Sivaguru, K. V. R. Keerthivaasan, B. R. Janaki, and R. Raffik, "Role of UAVs in innovating agriculture with future applications: A review," in *2021 International Conference on Advancements in Electrical, Electronics, Communication, Computing and Automation (ICAECA)*. IEEE, oct 2021.

[56] H. Ramirez-Rodriguez, V. Parra-Vega, A. Sanchez, and O. Garcia, "Integral sliding mode backstepping control of quadrotors for robust position tracking," in *2013 International Conference on Unmanned Aircraft Systems (ICUAS)*. IEEE, may 2013.

[57] K. Röbenack, "Computation of multiple lie derivatives by algorithmic differentiation," *Journal of Computational and Applied Mathematics*, vol. 213, no. 2, pp. 454–464, apr 2008.

[58] G. P. Rible, N. A. Arriola, and M. R. Jr., "Modeling and implementation of quadcopter autonomous flight based on alternative methods to determine propeller parameters," *Advances in Science, Technology and Engineering Systems Journal*, vol. 5, no. 5, pp. 727–741, 2020.

[59] L. E. Romero, D. F. Pozo, and J. A. Rosales, "Quadcopter stabilization by using pid controllers," *Maskana*, vol. 5, pp. 175–186, 2014.

[60] N. M. Salma and K. Osman, "Modelling and pid control system integration for quadcopter dji f450 attitude stabilization," *Indonesian Journal of Electrical Engineering and Computer Science*, vol. 19, no. 3, p. 1235, sep 2020.

[61] D. Schoenwald and . Özgüner, "The relative degree enhancement problem for mimo nonlinear systems," *IFAC Proceedings Volumes*, vol. 28, no. 14, pp. 287–291, jun 1995.

[62] R. Seifried, *Dynamics of Underactuated Multibody Systems: Modeling, Control and Optimal Design*, ser. Solid Mechanics and Its Applications. Springer International Publishing, 2013. [Online]. Available: https://books.google.de/books?id=91a6BAAAQBAJ

[63] J. Seo, R. Venugopal, and J.-P. Kenné, "Feedback linearization based control of a rotational hydraulic drive," *Control Engineering Practice*, vol. 15, no. 12, pp. 1495–1507, dec 2007.

[64] M. K. Shaik and J. F. Whidborne, "Robust sliding mode control of a quadrotor," in *2016 UKACC 11th International Conference on Control (CONTROL)*. IEEE, aug 2016.

[65] R. Sharma and D. Ghose, "Swarm intelligence based collision avoidance between realistically modelled UAV clusters," in *2007 American Control Conference*. IEEE, jul 2007.

[66] Z. Shulong, A. Honglei, Z. Daibing, and S. Lincheng, "A new feedback linearization LQR control for attitude of quadrotor," in *2014 13th International Conference on Control Automation Robotics & Vision (ICARCV)*. IEEE, dec 2014.

[67] J. Slotine and W. Li, *Applied Nonlinear Control*. Prentice Hall, 1991. [Online]. Available: https://books.google.de/books?id=cwpRAAAAMAAJ

[68] S. K. Srivastava, K. P. Seng, L. M. Ang, A. N. A. Pachas, and T. Lewis, "Drone-based environmental monitoring and image processing approaches for resource estimates of private native forest," *Sensors*, vol. 22, no. 20, p. 7872, oct 2022.

[69] B. Stevens, F. Lewis, and E. Johnson, *Aircraft Control and Simulation: Dynamics, Controls Design, and Autonomous Systems*. Wiley, 2015. [Online]. Available: https://books.google.de/books?id=lvhcCgAAQBAJ

[70] F. Szabo, *Linear Algebra with Mathematica: An Introduction Using Mathematica*. Elsevier Science, 2000. [Online]. Available: https://books.google.de/books?id=aqruCh5Hb2cC

[71] D. A. Tesch, D. Eckhard, and W. C. Guarienti, "Pitch and roll control of a quadcopter using cascade iterative feedback tuning," *IFAC-PapersOnLine*, vol. 49, no. 30, pp. 30–35, 2016.

[72] E. R. Vivoni, A. Rango, C. A. Anderson, N. A. Pierini, A. P. Schreiner-McGraw, S. Saripalli, and A. S. Laliberte, "Ecohydrology with unmanned aerial vehicles," *Ecosphere*, vol. 5, no. 10, p. art130, oct 2014.

[73] L. Wang and Q.-L. p Wang, "The feedback linearization based on backstepping technique," in *2009 IEEE International Conference on Intelligent Computing and Intelligent Systems*. IEEE, nov 2009.

[74] J. Willkomm, K. Wulff, and J. Reger, "Tracking-control for the boost-pressure of a turbo-charger based on a local model network," in *2019 IEEE International Conference on Mechatronics (ICM)*. IEEE, 2019.

[75] ——, "Quantitative robustness analysis of model following control for nonlinear systems subject to model uncertainties," *IFAC-PapersOnLine*, vol. 54, no. 14, pp. 167–172, 2021.

[76] ——, "Set-point tracking for nonlinear systems subject to uncertainties using model-following control with a high-gain controller," in *2022 European Control Conference (ECC)*. IEEE, jul 2022.

[77] N. Xuan-Mung and S.-K. Hong, "Improved altitude control algorithm for quadcopter unmanned aerial vehicles," *Applied Sciences*, vol. 9, no. 10, p. 2122, may 2019.

[78] K. Young, V. Utkin, and U. Ozguner, "A control engineer's guide to sliding mode control," *IEEE Transactions on Control Systems Technology*, vol. 7, no. 3, pp. 328–342, may 1999.

[79] L. Yuan, H. Feng-you, and W. Feng, "Nominal model-based control for permanent magnet synchronous motor," in *2009 International Conference on Intelligent Human-Machine Systems and Cybernetics*. IEEE, 2009.

[80] Y. Zhang and A. Chamseddine, "Fault tolerant flight control techniques with application to a quadrotor uav testbed," *Automatic Flight Control Systems-Latest Developments*, vol. 6, no. 3, pp. 119–121, 2012.

[81] Y. Zhang, Y. Tan, Y. Onda, A. Hashimoto, T. Gomi, C. Chiu, and S. Inokoshi, "A tree detection method based on trunk point cloud section in dense plantation forest using drone LiDAR data," *Forest Ecosystems*, vol. 10, p. 100088, 2023.

[82] J. Zheng and P. Li, "Backstepping control for a quadrotor based on the structure of inner and outer loops," in *2018 Chinese Control And Decision Conference (CCDC)*. IEEE, jun 2018.

[83] L. Zhou and B. Zhang, "Quadrotor UAV flight control using backstepping adaptive controller," in *2020 IEEE 6th International Conference on Control Science and Systems Engineering (ICCSSE)*. IEEE, jul 2020.